

# Heavy Quarkonium Hybrids: Spectrum, Decay and Mixing

Ruben Oncala<sup>1</sup> and Joan Soto<sup>2</sup>

<sup>1</sup>*Nikhef, Science Park 105, 1098 XG Amsterdam, The Netherland*

<sup>2</sup>*Departament de Física Quàntica i Astrofísica and Institut de Ciències del Cosmos, Universitat de Barcelona, Martí i Franquès 1, 08028 Barcelona, Catalonia, Spain*

(Dated: July 12, 2017)

We present a largely model independent analysis of the lighter Heavy Quarkonium Hybrids based on the strong coupling regime of Potential Non-Relativistic QCD (pNRQCD). We calculate the spectrum at leading order, including the mixing of static hybrid states. We use potentials that fulfill the required short and long distance theoretical constraints and fit well the available lattice data. We argue that the decay width to the lower lying Heavy Quarkonia can be reliably estimated in some cases, and provide results for a selected set of decays. We also consider the mixing with Heavy Quarkonium states. We establish the form of the mixing potential at  $O(1/m_Q)$ ,  $m_Q$  being the mass of the heavy quarks, and work out its short and long distance constraints. The weak coupling regime of pNRQCD and the effective string theory of QCD are used for that goal. We show that the mixing effects may indeed be important and produce large spin symmetry violations. Most of the isospin zero XYZ states fit well in our spectrum, either as a Hybrid or standard Quarkonium candidates.

PACS numbers: 14.40.Rt, 14.40.Pq, 13.25.Jx

## I. INTRODUCTION

The so called XYZ states in the charmonium and bottomonium spectrum do not fit in the usual potential model expectations (see [1] for a recent review). A number of models have been proposed to understand them, ranging from compact tetraquark states to just kinematical enhancements caused by the heavy-light meson pair thresholds. We explore here the possibility that some of these states correspond to heavy quarkonium hybrids in a QCD based approach. Since charm and bottom masses are much larger than the typical QCD scale  $\Lambda_{\text{QCD}}$ , Non-Relativistic QCD (NRQCD) [2, 3] can be used for these states. For instance, the spectroscopy of bottomonium hybrids has been studied in lattice NRQCD in [4] and the production of charmonium hybrids in  $B$  decays in [5]. Furthermore, if we focus on a region of the spectrum much smaller than  $\Lambda_{\text{QCD}}$ , we should be able to build an effective theory in that region, by integrating out  $\Lambda_{\text{QCD}}$ , in a way similar to the strong coupling regime of Potential NRQCD (pNRQCD)[6]. The static limit is relevant for such a construction and the spectrum in that limit is known from lattice QCD in the case of  $n_f = 0$  (no light quarks) [7]. In the Born-Oppenheimer (BO) approximation, each energy level in the static case plays the role of a potential in a Schrödinger equation for the dynamical states build on that static energy level [8]. The static spectrum is displayed in fig. 1.

The ground state corresponds to the potential for heavy quarkonium states ( $\Sigma_g^+$ ), namely the one that it is usually input in potential models. The higher levels correspond to gluonic excitations and are called hybrid potentials. If we are interested in states of a certain energy, we must in principle take into account all the potentials below that energy, since the

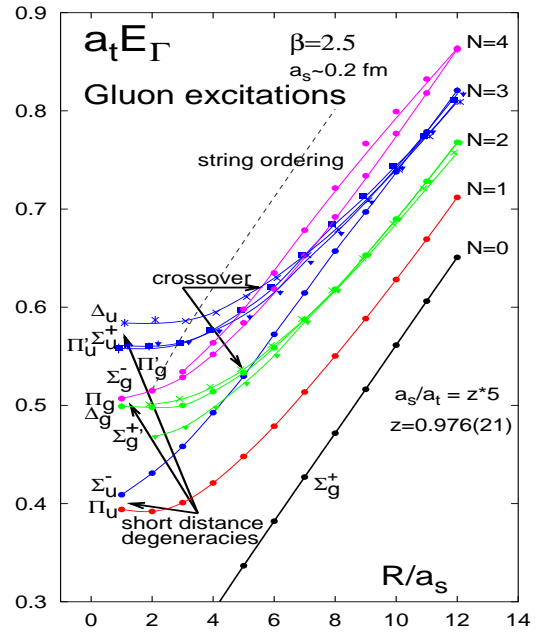


FIG. 1. Energy spectrum in the static limit for  $n_f = 0$  [7].

states build on different potentials may influence each other through  $1/m_Q$  corrections,  $m_Q$  being the mass of the heavy quarks ( $Q = c, b$ ). We shall focus here on the lower lying hybrid states built out of  $\Pi_u$  and  $\Sigma_u^-$ . In addition to calculating the spectrum [4, 9, 10], we will address the question on how they interact with quarkonium, namely with the states build out of  $\Sigma_g^+$ .

The quarkonium states far below the energy of the hybrid states can be integrated out and may contribute to the decay width, whereas the quarkonium states in the same energy range as hybrid states may mix with them. We will learn that certain hybrid states do not decay to lower lying heavy quarkonium at leading order, and that the mixing with quarkonium may induce large spin symmetry violations. These observations will be instrumental to identify a number of XYZ states as hybrids. In fact, it turns out that most of the XYZ states can eventually be identified with either hybrids or quarkonium in our approach. Preliminary results have been reported in [11].

The rest of the paper is organized as follows. In Sec. II we calculate the spectrum of the lower lying hybrid states ignoring any possible mixing with other states. In Section III we argue that the decay width to lower lying quarkonia can be reliably estimated in some cases, and calculate it for a number of states. In Sec. IV, we address the mixing with quarkonium states. We establish the form of the mixing potential at  $\mathcal{O}(1/m_Q)$ , and derive the short and long distance constraints that it must fulfill using pNRQCD in the weak coupling regime [6, 12] and the effective string theory of QCD respectively [13, 14]. We explore several interpolations for the mixing potential and recalculate the spectrum. In Section V and Section VI we compare our results with those of other QCD based approaches and with the experiment respectively. We also present in the latter the most likely identifications of the XYZ states as hybrids or quarkonium. Section VII contains a discussion of our results. Finally, in Sec. VIII we present a short summary of the main results and conclude. Appendix A shows our results for quarkonium. Appendix B provides details on how we obtain the two long distance parameters from lattice data. Appendix C sets our conventions for the tensor spherical harmonics. The tables in Appendix D display our results for the full (quarkonium plus hybrid) charmonium and bottomonium spectrum including mixing.

## II. SPECTRUM

In the Born-Oppenheimer approximation, the calculation of the hybrid spectrum reduces to solving the Schrödinger equation with a potential  $V = V(r, \Lambda_{\text{QCD}})$  that has a minimum at  $r = r_0 \sim 1/\Lambda_{\text{QCD}}$ ,  $r = |\mathbf{r}|$ ,  $\mathbf{r}$  being the distance between the quark and the antiquark. Hence the energy of the small fluctuations about that minimum is  $E \sim \sqrt{\Lambda_{\text{QCD}}^3/m_Q} \ll \Lambda_{\text{QCD}} \ll m_Q$ . Consequently, we are in a situation analogous to the strong coupling regime of pNRQCD in which the scale  $\Lambda_{\text{QCD}}$  is integrated out. It then makes sense to restrict the study to the lower lying hybrid potentials,  $\Sigma_u^-$  and  $\Pi_u$ , since the gap to the

next states is parametrically  $O(\Lambda_{\text{QCD}})$ . Specifically, from Fig. 1 we see that the gap between the minimum of the  $\Pi_u$  potential and the first excited potential that we neglect ( $\Sigma_g^{+'}$ ) is about 400 MeV. Hence, for states built out of the  $\Sigma_u^-$  and  $\Pi_u$  potentials about 400 MeV or more above the lowest lying one, mixing effects with the next hybrid multiplet ( $\Sigma_g^+$ ,  $\Pi_g$ ,  $\Delta_g$ ) may be relevant.

The potentials associated to  $\Sigma_u^-$  and  $\Pi_u$  are generated at short distances. In weak coupling pNRQCD [12], this is easily understood as they correspond to different projections with respect to  $\mathbf{r}$  of the same operator  $\text{tr}(\mathbf{B}(\mathbf{0}, t)O(\mathbf{0}, \mathbf{r}, t))$ , where  $O(\mathbf{R}, \mathbf{r}, t)$  is the color octet operator,  $\mathbf{B}(\mathbf{R}, t)$  the chromomagnetic field, and we have set the center of mass coordinate  $\mathbf{R}=\mathbf{0}$ . These projections have well defined transformations under the  $D_{\infty h}$  group, the group of a diatomic molecule.  $\hat{\mathbf{r}}\mathbf{B}$  corresponds to  $\Sigma_u^-$  and  $\mathbf{B} - \hat{\mathbf{r}}(\hat{\mathbf{r}}\mathbf{B})$  to  $\Pi_u$  [6]. It is then natural to associate to the lower lying hybrids a vectorial wave function  $\mathbf{H}(\mathbf{0}, \mathbf{r}, t)$ , such that its projection to  $\mathbf{r}$  evolves with  $V_{\Sigma_u^-}$  and its projection orthogonal to  $\mathbf{r}$  with  $V_{\Pi_u}$ . We then have the following Lagrangian density,

$$\mathcal{L} = \text{tr} \left( H^{i\dagger} (\delta_{ij} i \partial_0 - h_{Hij}) H_j \right) \quad (1)$$

$$h_{Hij} = \left( -\frac{\nabla^2}{m_Q} + V_{\Sigma_u^-}(r) \right) \delta_{ij} + (\delta_{ij} - \hat{r}_i \hat{r}_j) \left[ V_{\Pi_u}(r) - V_{\Sigma_u^-}(r) \right],$$

where  $\hat{\mathbf{r}} = \mathbf{r}/|\mathbf{r}|$  and we have ignored the center of mass motion.  $\mathbf{H} = \mathbf{H}(\mathbf{R}, \mathbf{r}, t)$  is a matrix in spin space and transforms as  $\mathbf{H} \rightarrow h_1 \mathbf{H} h_2^\dagger$ ,  $h_1, h_2 \in SU(2)$  under spin symmetry.  $h_{Hij}$  above does not depend on the spin of the quarks, and hence it is invariant under spin symmetry transformations, but it does depend on the total angular momentum of the gluonic degrees of freedom  $\mathbf{L}_g$ , in this case  $L_g = 1$  as it is apparent from the vectorial character of  $\mathbf{H}$ . The symmetry properties of  $\mathbf{H}(\mathbf{R}, \mathbf{r}, t)$  under parity, time reversal and charge conjugation read as follows,

$$\begin{aligned} P : \mathbf{H}(\mathbf{R}, \mathbf{r}, t) &\rightarrow -\mathbf{H}(-\mathbf{R}, -\mathbf{r}, t) \\ T : \mathbf{H}(\mathbf{R}, \mathbf{r}, t) &\rightarrow -\sigma^2 \mathbf{H}(\mathbf{R}, \mathbf{r}, -t) \sigma^2 \\ C : \mathbf{H}(\mathbf{R}, \mathbf{r}, t) &\rightarrow -\sigma^2 \mathbf{H}^T(\mathbf{R}, -\mathbf{r}, t) \sigma^2, \end{aligned} \quad (2)$$

where  $\sigma^2$  is the second Pauli matrix. Hence the  $P$  and  $C$  associated to a Hybrid state with quark-antiquark orbital angular momentum  $L$  and quark-antiquark spin  $S$  become,

$$P = (-1)^{L+1}, \quad C = (-1)^{L+S+1}. \quad (3)$$

Leaving aside the spin of the quarks, it is convenient to express  $\mathbf{H}$  in a basis of eigenfunctions of  $\mathbf{J} = \mathbf{L} + \mathbf{L}_g$ , where  $\mathbf{L}$  is the orbital angular momentum of the quarks. This is achieved using Vector Spherical

Harmonics [15],

$$\mathbf{H}(\mathbf{r}) = \frac{1}{r} \left( P_0^+(r) \mathbf{Y}_{00}^{L=1} + \sum_{J=1}^{\infty} \sum_{M=-J}^J [P_J^+(r) \mathbf{Y}_{JM}^{L=J+1} + P_J^0(r) \mathbf{Y}_{JM}^{L=J} + P_J^-(r) \mathbf{Y}_{JM}^{L=|J-1|}] \right). \quad (4)$$

Note that  $\mathbf{J}$  is a conserved quantity thanks to heavy quark spin symmetry.  $\mathbf{Y}_{JM}^L = \mathbf{Y}_{JM}^L(\theta, \phi)$  fulfil,

$$\begin{aligned} \mathbf{J}^2 \mathbf{Y}_{JM}^L &= J(J+1) \mathbf{Y}_{JM}^L, & \mathbf{L}^2 \mathbf{Y}_{JM}^L &= L(L+1) \mathbf{Y}_{JM}^L, \\ \mathbf{L}_g^2 \mathbf{Y}_{JM}^L &= 2 \mathbf{Y}_{JM}^L, & J_3 \mathbf{Y}_{JM}^L &= M \mathbf{Y}_{JM}^L. \end{aligned} \quad (5)$$

The eigenvalue problem then reduces for  $J \neq 0$  to

$$V_q(r) \begin{pmatrix} -\frac{1}{m_Q} \frac{\partial^2}{\partial r^2} + \begin{pmatrix} \frac{(J-1)J}{m_Q r^2} & 0 \\ 0 & \frac{(J+1)(J+2)}{m_Q r^2} \end{pmatrix} + V_{\Sigma_u^-}(r) \\ \frac{J+1}{2J+1} & \frac{\sqrt{(J+1)J}}{2J+1} \\ \frac{\sqrt{(J+1)J}}{2J+1} & \frac{J}{2J+1} \end{pmatrix} \begin{pmatrix} P_J^-(r) \\ P_J^+(r) \end{pmatrix} = E \begin{pmatrix} P_J^-(r) \\ P_J^+(r) \end{pmatrix}$$

$$\left( -\frac{1}{m_Q} \frac{\partial^2}{\partial r^2} + \frac{J(J+1)}{m_Q r^2} + V_{\Pi_u}(r) \right) P_J^0(r) = E P_J^0(r), \quad (6)$$

where  $V_q(r) = V_{\Pi_u}(r) - V_{\Sigma_u^-}(r)$ , and for  $J = 0$  to

$$\left( -\frac{1}{m_Q} \frac{\partial^2}{\partial r^2} + \frac{2}{m_Q r^2} + V_{\Sigma_u^-}(r) \right) P_0^+(r) = E P_0^+(r). \quad (7)$$

The equations above are equivalent to those obtained in ref. [10]. We approximate  $V_{\Pi_u}(r)$  and  $V_{\Sigma_u^-}(r)$  by simple functions that have the correct behavior at short and long distances, and fit well the lattice results in fig 1 [7] and ref. [16]. For  $V_{\Sigma_u^-}(r)$  it is enough to take a Cornell-like potential with the correct asymptotic behavior in order to get a good fit to data. We then take,

$$V_{\Sigma_u^-}(r) = \frac{\sigma_s}{r} + \kappa_s r + E_s^{Q\bar{Q}}. \quad (8)$$

The correct short and long distance behavior implies  $\sigma_s = \sigma_g/8$  and  $\kappa_s = \kappa_g$ , where  $\sigma_g$  and  $\kappa_g$  are the corresponding parameters appearing in the Cornell potential for heavy quarkonium ( $V_{\Sigma_g^+}(r)$ ), see Appendix A. We then have,

$$\sigma_s = 0.061, \quad \kappa_s = 0.187 \text{ GeV}^2. \quad (9)$$

The constant  $E_s^{Q\bar{Q}}$  becomes then the only free parameter, which can be linked to the corresponding parameter for the heavy quarkonium case,  $E_g^{Q\bar{Q}}$  through the lattice data of ref. [7]. Finally,  $E_g^{Q\bar{Q}}$  is obtained in Appendix A by fitting the heavy quarkonium spectrum. We get,

$$E_s^{c\bar{c}} = 0.559 \text{ GeV}, \quad E_s^{b\bar{b}} = 0.573 \text{ GeV}. \quad (10)$$

For  $V_{\Pi_u}(r)$  a Cornell-like form does not fit lattice data well at intermediate distances. Hence, we take a slightly more complicated form for it,

$$V_{\Pi_u}(r) = \frac{\sigma_p}{r} \left( \frac{1 + b_1 r + b_2 r^2}{1 + a_1 r + a_2 r^2} \right) + \kappa_p r + E_p^{Q\bar{Q}}. \quad (11)$$

At short distances this potential must coincide with  $V_{\Sigma_u^-}(r)$  up to terms that vanish when  $r \rightarrow 0$  [6]. This implies  $\sigma_p = \sigma_s$  and  $E_p^{Q\bar{Q}} - E_s^{Q\bar{Q}} + \sigma_p(b_1 - a_1) = 0$ . At long distances it must be consistent with the effective string theory of QCD [14],

$$E_N(r \rightarrow \infty) = \kappa r + (\pi N - \frac{(D-2)\pi}{24}) \frac{1}{r} + O(1/r^2), \quad (12)$$

where  $D$  is the space-time dimension and  $N$  labels the energy spectrum of the string. The leading term of this formula implies  $\kappa_p = \kappa_s = \kappa$ . The next-to-leading term provides the extra constraint,

$$2\pi - \sigma_s + \frac{\sigma_p b_2}{a_2} = 0, \quad (13)$$

which follows from Fig. 1 [7]. Indeed those data show the non-trivial fact that the  $V_{\Pi_u}(r)$  and  $V_{\Sigma_u^-}(r)$  potentials at long distances correspond to the  $N = 1$  and  $N = 3$  string energy levels respectively. Putting together all the constraints above allows to solve  $a_1$ ,  $b_1$  and  $b_2$  as a function of known parameters, and  $E_p^{Q\bar{Q}}$  and  $a_2$ , which are fitted to lattice data. We obtain,

$$\begin{aligned} \sigma_p &= 0.061, & \kappa_p &= 0.187 \text{ GeV}^2 \\ b_1 &= 0.06964 \text{ GeV}, & b_2 &= -1.45934 \text{ GeV}^2 \\ a_1 &= -0.06733 \text{ GeV}, & a_2 &= 0.01433 \text{ GeV}^2 \\ E_p^{c\bar{c}} &= 0.551 \text{ GeV}, & E_p^{b\bar{b}} &= 0.565 \text{ GeV}. \end{aligned} \quad (14)$$

The central value of lattice data and the outcome of the fits above are shown in fig. 2, together with the potential for quarkonium  $V_{\Sigma_g^+}$  discussed in the Appendix A.

Using the potentials above as an input we solve (6-7) and obtain the results displayed in tables I and II in terms of  $M_{Q\bar{Q}g} = 2m_Q + E$ . Details on the code used can be found in [17]. We have also displayed the results in Figs. 3 and 4, where we have included the errors discussed at the end of Sec. IV C.

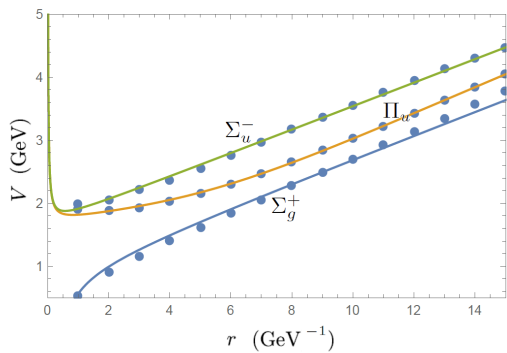


FIG. 2. Our fits to the lattice results of ref. [7] for the three lower lying B-O potentials  $V_{\Sigma_g^+}$ ,  $V_{\Pi_u}$  and  $V_{\Sigma_u^-}$ .

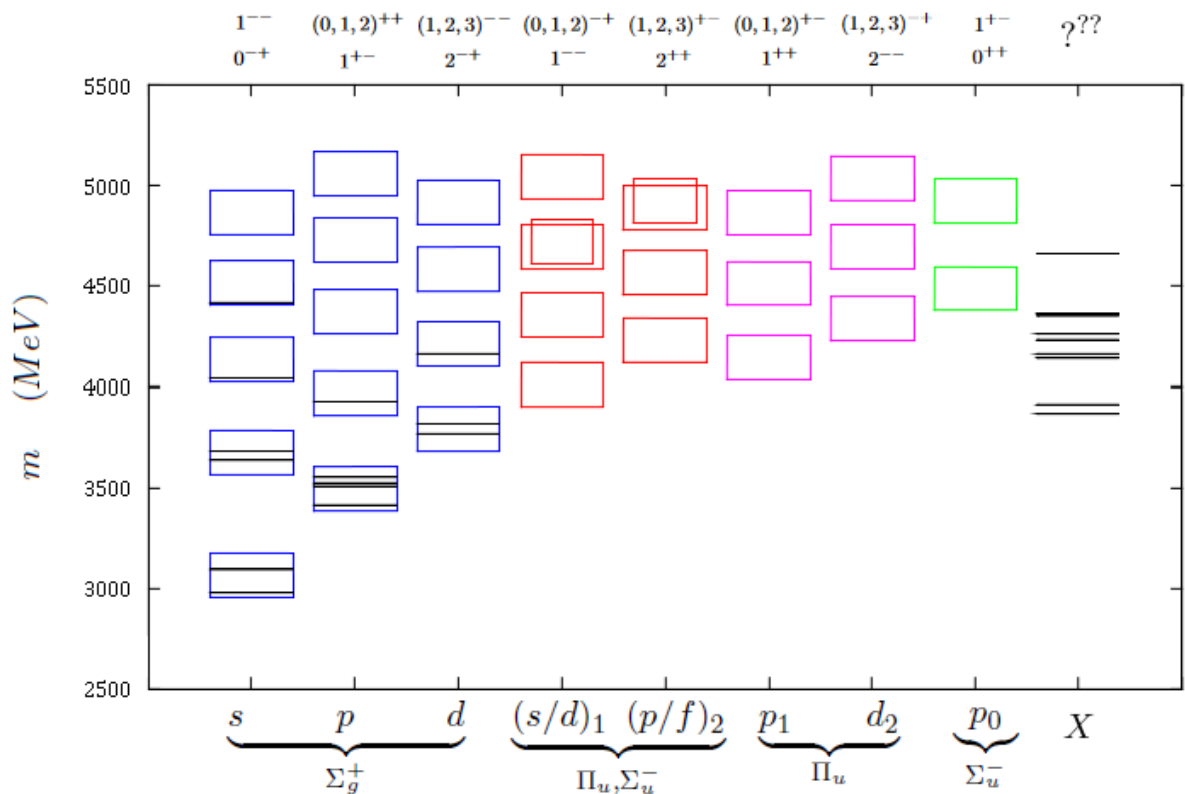


FIG. 3. Charmonium spectrum in Table I. The height of the boxes corresponds to the error estimated at the end of Sec. IV C. The states identified as quarkonium in the PDG [37] are displayed in the corresponding column, whereas the states labeled as  $X$  in the PDG [37] are displayed in a separated column. The box assignment of the latter is discussed in Sec. VI.

### III. DECAY

Since we are interested in the lower lying hybrid states, it is enough for us to consider an effective theory for energy fluctuations much smaller than  $\Lambda_{\text{QCD}}$  around those states. The energy gap to the lower ly-

ing quarkonium states is greater than  $\Lambda_{\text{QCD}}$ . Hence those states can be integrated out, which will give rise to an imaginary potential  $\Delta V$ , which in turn will produce the semi-inclusive decay width for a hybrid state to decay into any quarkonium state,  $\Gamma_{H_m \rightarrow S} = -2 \langle H_m | \text{Im} \Delta V | H_m \rangle$ . This is much in the same way as

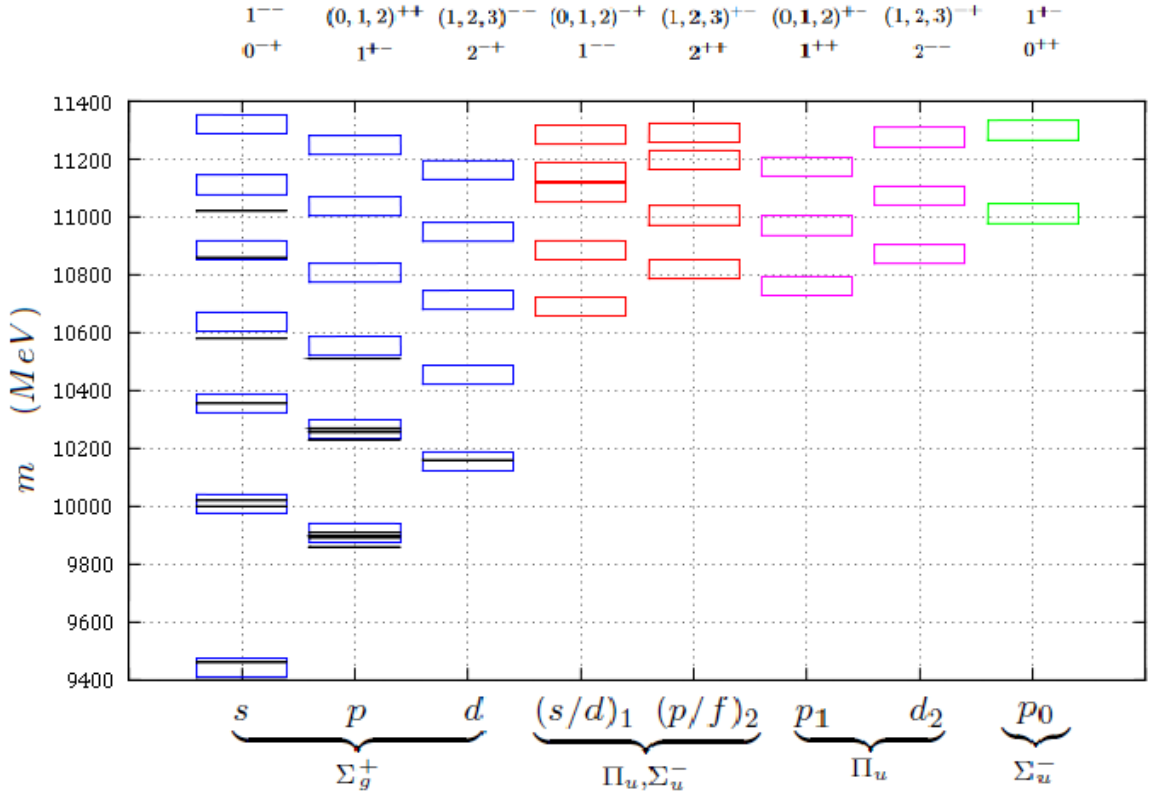


FIG. 4. Bottomonium spectrum in Table II. The height of the boxes corresponds to the error estimated at the end of Sec. IV C. The states identified as quarkonium in the PDG [37] are displayed in the corresponding column.

integrating out hard gluons in QCD produces operators with imaginary matching coefficients in NRQCD [3], which give rise to the total decay width of a given quarkonium state to light degrees of freedom. Furthermore, if we assume that the energy gap to a given quarkonium state  $S_n$ ,  $\Delta E_{mn}$ , fulfils  $\Delta E_{mn} \gg \Lambda_{\text{QCD}}$ , and that the process is short distance dominated, the integration for that state can be done using the weak coupling regime of pNRQCD [6, 12],

$$\begin{aligned} \mathcal{L}_{p\text{NRQCD}} = & \text{Tr} \left\{ S^\dagger (i\partial_0 - h_s) S + O^\dagger (iD_0 - h_o) O \right\} \\ & + \text{Tr} \left\{ O^\dagger \mathbf{r} \cdot g\mathbf{E} S + \text{H.c.} + \frac{O^\dagger \mathbf{r} \cdot g\mathbf{E} O}{2} + \frac{O^\dagger O \mathbf{r} \cdot g\mathbf{E}}{2} \right\} \\ & + \dots \end{aligned} \quad (15)$$

The singlet field  $S$  encodes the quarkonium states whereas the octet field  $O$  encodes the heavy quark content of the hybrid states,  $h_s$  and  $h_o$  are Hamiltonians containing the respective Coulomb-type potentials and  $\mathbf{E} = \mathbf{E}(\mathbf{R}, t)$  is the chromoelectric field (see [18] for details). The leading contribution corresponds to the diagram in fig. 5. We obtain,

$$\text{Im}\Delta V = -\frac{2}{3} \frac{\alpha_s T_F}{N_c} \sum_n r^i |S_n\rangle \langle S_n| r^i (i\partial_t - E_n)^3, \quad (16)$$

$T_F = 1/2$ ,  $N_c = 3$ , and  $\alpha_s = g^2/4\pi$  is the QCD strong coupling constant.  $E_n$  is the energy of the  $n$ -th quarkonium state,  $S_n$ .

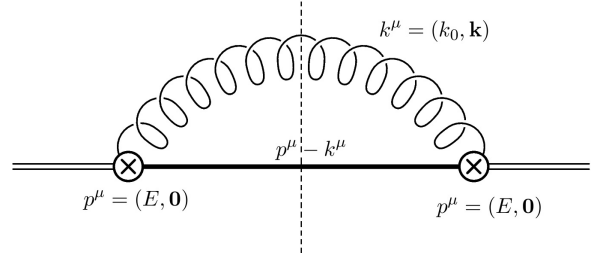


FIG. 5. The octet field self-energy diagram in weak coupling pNRQCD [18]. Double line represents the octet propagator, while single lines represent the singlet propagator. The curly line stands for the gluon propagator and the crossed circles for chromoelectric dipole vertices. The expectator gluons that make up the physical state together with the octet field are not displayed.

From the expression above, we identify

$$\Gamma(H_m \rightarrow S_n) = \frac{4\alpha_s T_F}{3 N_c} \langle H_m | r^i | S_n \rangle \langle S_n | r^i | H_m \rangle \Delta E_{mn}^3. \quad (17)$$

$NL_J$	w-f	$M_{c\bar{c}}$	$M_{c\bar{c}g}$	$S=0$ $\mathcal{J}^{PC}$	$S=1$ $\mathcal{J}^{PC}$	$\Lambda_\eta^\epsilon$
1s	S	3068		$0^{-+}$	$1^{--}$	$\Sigma_g^+$
2s	S	3678		$0^{-+}$	$1^{--}$	$\Sigma_g^+$
3s	S	4131		$0^{-+}$	$1^{--}$	$\Sigma_g^+$
1p <sub>0</sub>	$P^+$		4486	$0^{++}$	$1^{+-}$	$\Sigma_u^-$
4s	S	4512		$0^{-+}$	$1^{--}$	$\Sigma_g^+$
2p <sub>0</sub>	$P^+$		4920	$0^{++}$	$1^{+-}$	$\Sigma_u^-$
3p <sub>0</sub>	$P^+$		5299	$0^{++}$	$1^{+-}$	$\Sigma_u^-$
4p <sub>0</sub>	$P^+$		5642	$0^{++}$	$1^{+-}$	$\Sigma_u^-$
1p	S	3494		$1^{+-}$	$(0, 1, 2)^{++}$	$\Sigma_g^+$
2p	S	3968		$1^{+-}$	$(0, 1, 2)^{++}$	$\Sigma_g^+$
1(s/d) <sub>1</sub>	$P^{+-}$		4011	$1^{--}$	$(0, 1, 2)^{-+}$	$\Pi_u \Sigma_u^-$
1p <sub>1</sub>	$P^0$		4145	$1^{++}$	$(0, 1, 2)^{-+}$	$\Pi_u$
2(s/d) <sub>1</sub>	$P^{+-}$		4355	$1^{--}$	$(0, 1, 2)^{-+}$	$\Pi_u \Sigma_u^-$
3p	S	4369		$1^{+-}$	$(0, 1, 2)^{++}$	$\Sigma_g^+$
2p <sub>1</sub>	$P^0$		4511	$1^{++}$	$(0, 1, 2)^{-+}$	$\Pi_u$
3(s/d) <sub>1</sub>	$P^{+-}$		4692	$1^{--}$	$(0, 1, 2)^{-+}$	$\Pi_u \Sigma_u^-$
4(s/d) <sub>1</sub>	$P^{+-}$		4718	$1^{--}$	$(0, 1, 2)^{-+}$	$\Pi_u \Sigma_u^-$
4p	S	4727		$1^{+-}$	$(0, 1, 2)^{++}$	$\Sigma_g^+$
3p <sub>1</sub>	$P^0$		4863	$1^{++}$	$(0, 1, 2)^{-+}$	$\Pi_u$
5(s/d) <sub>1</sub>	$P^{+-}$		5043	$1^{--}$	$(0, 1, 2)^{-+}$	$\Pi_u \Sigma_u^-$
5p	S	5055		$1^{+-}$	$(0, 1, 2)^{++}$	$\Sigma_g^+$
1d	S	3793		$2^{-+}$	$(1, 2, 3)^{-}$	$\Sigma_g^+$
2d	S	4210		$2^{-+}$	$(1, 2, 3)^{-}$	$\Sigma_g^+$
1(p/f) <sub>2</sub>	$P^{+-}$		4231	$2^{++}$	$(1, 2, 3)^{-}$	$\Pi_u \Sigma_u^-$
1d <sub>2</sub>	$P^0$		4334	$2^{--}$	$(1, 2, 3)^{-}$	$\Pi_u$
2(p/f) <sub>2</sub>	$P^{+-}$		4563	$2^{++}$	$(1, 2, 3)^{-}$	$\Pi_u \Sigma_u^-$
3d	S	4579		$2^{-+}$	$(1, 2, 3)^{-}$	$\Sigma_g^+$
2d <sub>2</sub>	$P^0$		4693	$2^{--}$	$(1, 2, 3)^{-}$	$\Pi_u$
3(p/f) <sub>2</sub>	$P^{+-}$		4886	$2^{++}$	$(1, 2, 3)^{-}$	$\Pi_u \Sigma_u^-$
4d	S	4916		$2^{-+}$	$(1, 2, 3)^{-}$	$\Sigma_g^+$
4(p/f) <sub>2</sub>	$P^{+-}$		4923	$2^{++}$	$(1, 2, 3)^{-}$	$\Pi_u \Sigma_u^-$
3d <sub>2</sub>	$P^0$		5036	$2^{--}$	$(1, 2, 3)^{-}$	$\Pi_u$

TABLE I. Charmonium (S) and hybrid charmonium ( $P^{+-0}$ ) energy spectrum computed with  $m_c = 1.47GeV$ . Masses are in MeV. States which only differ by the heavy quark spin ( $S = 0, 1$ ) are degenerated.  $N$  is the principal quantum number,  $L$  the orbital angular momentum of the heavy quarks,  $J$  is  $L$  plus the total angular momentum of the gluons,  $S$  the spin of the heavy quarks and  $\mathcal{J}$  is the total angular momentum. For quarkonium,  $J$  coincides with  $L$  and it is not displayed. The last column shows the relevant potentials for each state. The  $(s/d)_1$ ,  $p_1$ ,  $p_0$ ,  $(p/f)_2$  and  $d_2$  states are named  $H_1$ ,  $H_2$ ,  $H_3$ ,  $H_4$  and  $H_5$  respectively in [10].

$\Delta E_{mn} = E_m - E_n$ ,  $E_m$  being the energy of the hybrid state. At this order, the decays respect heavy quark spin symmetry, and hence the spin of the heavy quarks must be the same in the initial hybrid state and in the final quarkonium state. In addition, a selection rule derived from this formula is that hybrid states with

$NL_J$	w-f	$M_{b\bar{b}}$	$M_{b\bar{b}g}$	$S=0$ $\mathcal{J}^{PC}$	$S=1$ $\mathcal{J}^{PC}$	$\Lambda_\eta^\epsilon$
1s	S	9442		$0^{-+}$	$1^{--}$	$\Sigma_g^+$
2s	S	10009		$0^{-+}$	$1^{--}$	$\Sigma_g^+$
3s	S	10356		$0^{-+}$	$1^{--}$	$\Sigma_g^+$
4s	S	10638		$0^{-+}$	$1^{--}$	$\Sigma_g^+$
1p <sub>0</sub>	$P^+$		11011	$0^{++}$	$1^{+-}$	$\Sigma_u^-$
2p <sub>0</sub>	$P^+$		11299	$0^{++}$	$1^{+-}$	$\Sigma_u^-$
3p <sub>0</sub>	$P^+$		11551	$0^{++}$	$1^{+-}$	$\Sigma_u^-$
4p <sub>0</sub>	$P^+$		11779	$0^{++}$	$1^{+-}$	$\Sigma_u^-$
1p	S	9908		$1^{+-}$	$(0, 1, 2)^{++}$	$\Sigma_g^+$
2p	S	10265		$1^{+-}$	$(0, 1, 2)^{++}$	$\Sigma_g^+$
3p	S	10553		$1^{+-}$	$(0, 1, 2)^{++}$	$\Sigma_g^+$
1(s/d) <sub>1</sub>	$P^{+-}$		10690	$1^{--}$	$(0, 1, 2)^{-+}$	$\Pi_u \Sigma_u^-$
1p <sub>1</sub>	$P^0$		10761	$1^{++}$	$(0, 1, 2)^{-+}$	$\Pi_u$
4p	S	10806		$1^{+-}$	$(0, 1, 2)^{++}$	$\Sigma_g^+$
2(s/d) <sub>1</sub>	$P^{+-}$		10885	$1^{--}$	$(0, 1, 2)^{-+}$	$\Pi_u \Sigma_u^-$
2p <sub>1</sub>	$P^0$		10970	$1^{++}$	$(0, 1, 2)^{-+}$	$\Pi_u$
5p	S	11035		$1^{+-}$	$(0, 1, 2)^{++}$	$\Sigma_g^+$
3(s/d) <sub>1</sub>	$P^{+-}$		11084	$1^{--}$	$(0, 1, 2)^{-+}$	$\Pi_u \Sigma_u^-$
4(s/d) <sub>1</sub>	$P^{+-}$		11156	$1^{--}$	$(0, 1, 2)^{-+}$	$\Pi_u \Sigma_u^-$
3p <sub>1</sub>	$P^0$		11175	$1^{++}$	$(0, 1, 2)^{-+}$	$\Pi_u$
6p	S	11247		$1^{+-}$	$(0, 1, 2)^{++}$	$\Sigma_g^+$
5(s/d) <sub>1</sub>	$P^{+-}$		11284	$1^{--}$	$(0, 1, 2)^{-+}$	$\Pi_u \Sigma_u^-$
1d	S	10155		$2^{-+}$	$(1, 2, 3)^{-}$	$\Sigma_g^+$
2d	S	10454		$2^{-+}$	$(1, 2, 3)^{-}$	$\Sigma_g^+$
3d	S	10712		$2^{-+}$	$(1, 2, 3)^{-}$	$\Sigma_g^+$
1(p/f) <sub>2</sub>	$P^{+-}$		10819	$2^{++}$	$(1, 2, 3)^{-}$	$\Pi_u \Sigma_u^-$
1d <sub>2</sub>	$P^0$		10870	$2^{--}$	$(1, 2, 3)^{-}$	$\Pi_u$
4d	S	10947		$2^{-+}$	$(1, 2, 3)^{-}$	$\Sigma_g^+$
2(p/f) <sub>2</sub>	$P^{+-}$		11005	$2^{++}$	$(1, 2, 3)^{-}$	$\Pi_u \Sigma_u^-$
2d <sub>2</sub>	$P^0$		11074	$2^{--}$	$(1, 2, 3)^{-}$	$\Pi_u$
5d	S	11163		$2^{-+}$	$(1, 2, 3)^{-}$	$\Sigma_g^+$
3(p/f) <sub>2</sub>	$P^{+-}$		11197	$2^{++}$	$(1, 2, 3)^{-}$	$\Pi_u \Sigma_u^-$
3d <sub>2</sub>	$P^0$		11275	$2^{--}$	$(1, 2, 3)^{-}$	$\Pi_u$
4(p/f) <sub>2</sub>	$P^{+-}$		11291	$2^{++}$	$(1, 2, 3)^{-}$	$\Pi_u \Sigma_u^-$

TABLE II. Bottomonium (S) and hybrid bottomonium ( $P^{+-0}$ ) energy spectrum computed with  $m_b = 4.88GeV$ . Masses are in MeV. States which only differ by the heavy quark spin ( $S = 0, 1$ ) are degenerated.  $N$  is the principal quantum number,  $L$  the orbital angular momentum of the heavy quarks,  $J$  is  $L$  plus the total angular momentum of the gluons,  $S$  the spin of the heavy quarks and  $\mathcal{J}$  is the total angular momentum. For quarkonium,  $J$  coincides with  $L$  and it is not displayed. The last column shows the relevant potentials for each state. The  $(s/d)_1$ ,  $p_1$ ,  $p_0$ ,  $(p/f)_2$  and  $d_2$  states are named  $H_1$ ,  $H_2$ ,  $H_3$ ,  $H_4$  and  $H_5$  respectively in [10].

$L = J$  do not decay to lower lying quarkonium. This selection rule will be instrumental later on to select hybrid candidates among competing XYZ states. For the allowed decays, the numerical values of the decay widths are given in table III. We have only displayed numbers that can be reliably estimated, namely that  $\Delta E_{mn}$  is large enough and that  $\langle H_m | r^i | S_n \rangle$  is small enough so that the weak coupling regime of pNRQCD is sensible, see the table caption for details. We have taken the energies and wave functions for quarkonium and for hybrids from Appendix A and from the previous section respectively. The errors account for the fact that the quarkonium spectrum in (16) is meant to be calculated in the weak coupling regime (Coulomb type bound states) whereas we actually use in (17) the one in the strong coupling regime.

$NL_J \rightarrow N'L'$	$\Delta E$	$\langle r \rangle_{mn}$	$ \Delta E \langle r \rangle_{mn} $	$\alpha_s(\Delta E)$	$\Gamma$ (MeV)
$1p_0 \rightarrow 2s$	808	0.40	0.32	0.41	7.5(7.4)
$2(s/d)_1 \rightarrow 1p$	861	0.63	0.54	0.39	22(19)
$4(s/d)_1 \rightarrow 1p$	1224	0.42	0.51	0.33	23(15)
$1p_0 \rightarrow 1s$	1569	-0.42	0.65	0.29	44(23)
$1p_0 \rightarrow 2s$	1002	0.43	0.43	0.36	15(9)
$2p_0 \rightarrow 2s$	1290	-0.14	0.18	0.32	2.9(1.3)
$2p_0 \rightarrow 3s$	943	0.46	0.44	0.37	15(12)
$4p_0 \rightarrow 1s$	2337	0.27	0.63	0.25	53(25)
$4p_0 \rightarrow 2s$	1770	0.23	0.40	0.28	18(7)
$4p_0 \rightarrow 3s$	1423	0.19	0.28	0.31	7.4(4.1)
$2(s/d)_1 \rightarrow 1p$	977	0.47	0.46	0.37	17(8)
$3(s/d)_1 \rightarrow 1p$	1176	0.49	0.58	0.33	29(14)
$3(s/d)_1 \rightarrow 2p$	818	0.32	0.26	0.40	5(3)
$4(s/d)_1 \rightarrow 2p$	891	-0.74	0.66	0.39	33(25)
$5(s/d)_1 \rightarrow 1p$	1376	-0.31	0.43	0.31	18(7)
$5(s/d)_1 \rightarrow 2p$	1018	-0.41	0.42	0.36	14(8)

TABLE III. Decay widths for hybrid charmonium (above) and bottomonium (below) to lower lying charmonia and bottomonia respectively.  $m = NL_J$ ,  $n = N'L'$ ,  $\Delta E \equiv \Delta E_{mn}$  and  $\Gamma$  are in MeV, and  $\langle r \rangle_{mn}$  in  $\text{GeV}^{-1}$ .  $\alpha_s(\Delta E)$  is the one-loop running coupling constant at the scale  $\Delta E$ . We only display results for which  $\Delta E > 800\text{MeV}$  and  $|\Delta E \langle r \rangle_{mn}| < 0.7$ . The error (in brackets) includes higher orders in  $\alpha_s$  and in the multipole expansion, as well as the average of the linear term in the Cornell potential in order to account for the difference between weak and strong coupling regimes.

Model independent results for hybrid decays in the Born-Oppenheimer approximation have been obtained before in [19]. In that reference selection rules, based on the symmetries of the static limit, are obtained for a two-body decay of a hybrid to quarkonium plus a light meson, which constrain the possible quantum numbers of the latter. Our results are obtained under different assumptions, and may be regarded as complementary to those of ref. [19]. First of all, our results hold beyond the static limit (e.g.  $\Pi_u$ - $\Sigma_u^-$  mix-

ing is taken into account). Second, they are concerned with semi-inclusive decays, namely decays to quarkonium plus any state composed of light hadrons, rather than two-body decays. And third, they are based on the additional dynamical assumption that the decay process is short distance dominated. This assumption must be verified for each particular decay, and not always holds. In the cases it does, we are able to put forward not only constraints on quantum numbers (e.g.  $L$  must be different from  $J$  for a hybrid to decay to quarkonium) but also numerical estimates for the decay widths.

#### IV. MIXING

So far we have not taken into account the possible mixing of hybrid states with other states that are known to exist in the same energy range, like quarkonium or heavy-light meson pairs, which may distort the spectrum and the decay properties. We shall focus here on the effects in the spectrum of the mixing with quarkonium, basically because they are amenable to a systematic treatment. In the static limit, quarkonium (the lowest potential in fig. 1,  $\Sigma_g^+$ ) and heavy hybrids (the remaining potentials in fig. 1) do not mix by construction (they are built as orthogonal states). Hence, the mixing must be due to  $1/m_Q$  corrections to the Born-Oppenheimer approximation<sup>1</sup>. A way to systematically compute  $1/m_Q$  corrections for quarkonium was established in [20, 21] for the strong coupling regime of pNRQCD, following earlier work in the literature [22]. We show below how the formalism in [20] can also be used to calculate the mixing potentials. We may generally consider an effective theory for energy fluctuations  $E$  around a hybrid state, such that  $E \ll \Lambda_{\text{QCD}}$ . If there is a heavy quarkonium state close to that energy, we may expect it to modify the value of the energy  $E$ . This effective theory reads,

$$\begin{aligned} \mathcal{L}_{H+S} = & \text{tr} (S^\dagger [i\partial_0 - h_s] S) + \\ & + \text{tr} (H^{i\dagger} [i\delta_{ij}\partial_0 - h_{Hij}] H^j) + \\ & + \text{tr} (S^\dagger V_S^{ij} \{ \sigma^i, H^j \} + \text{H.c.}) . \end{aligned} \quad (18)$$

The traces are over spin indices and

$$V_S^{ij} = V_S^{ij}(\mathbf{r}) = \delta^{ij} V_S^\Pi(r) + \hat{r}^i \hat{r}^j (V_S^\Sigma(r) - V_S^\Pi(r)), \quad (19)$$

<sup>1</sup> In the weak coupling regime of pNRQCD, some  $\mathbf{p}/m_Q$  contributions can be reshuffled into  $\mathbf{r}i\partial_0$ , which have the same size, by local field redefinitions [6, 12, 18]. This is why singlet-octet transition terms appear in (15) with no apparent  $1/m_Q$  suppression.

is the mixing potential,  $h_s = -\frac{\nabla^2}{m_Q} + V_{\Sigma_g^+}(r)$  and  $h_{Hij}$  is defined in (1).  $S = S(\mathbf{R}, \mathbf{r}, t)$  transforms like  $\mathbf{H}$  under heavy quark spin symmetry and as follows under the discrete symmetries [18],

$$\begin{aligned} P : S(\mathbf{R}, \mathbf{r}, t) &\rightarrow -S(-\mathbf{R}, -\mathbf{r}, t) \\ T : S(\mathbf{R}, \mathbf{r}, t) &\rightarrow \sigma^2 S(\mathbf{R}, \mathbf{r}, -t) \sigma^2 \\ C : S(\mathbf{R}, \mathbf{r}, t) &\rightarrow \sigma^2 S^T(\mathbf{R}, -\mathbf{r}, t) \sigma^2. \end{aligned} \quad (20)$$

The transformations above together with those in (3) dictate the form of the last (mixing) term in (18). The form of  $V_S^{ij}(\mathbf{r})$  then follows from the symmetries of the static limit (see for instance [18]). Notice that in (18) we only include the  $1/m_Q$  corrections relevant to the mixing. There are also  $1/m_Q$  corrections to  $h_s$  [20] and to  $h_{Hij}$ , briefly discussed in Sec. VII, that we do not consider. For systems with the quark and antiquark of different flavor, two more terms are possible, which vanish in the equal mass limit,

$$\begin{aligned} \delta\mathcal{L}_{H+S} &= \text{tr} \left( S^\dagger V_S'^{ij} [\sigma^i, H^j] \right) + \\ &+ \text{tr} \left( S^\dagger V_L'^{ij} L^i H^j \right) + \text{H.c.}, \end{aligned} \quad (21)$$

where  $L^i$  is the angular momentum operator.

### A. Matching to NRQCD at $\mathcal{O}(1/m_Q)$

The NRQCD operators that create states at time  $t$  with the same quantum numbers as  $S$  and  $\mathbf{H}$  in the static limit read,

$$\begin{aligned} \hat{O}^\dagger(\mathbf{r}, \mathbf{R}, t) &\equiv \psi^\dagger\left(\frac{\mathbf{r}}{2}, t\right) W\left(\frac{\mathbf{r}}{2}, -\frac{\mathbf{r}}{2}; t\right) \chi\left(-\frac{\mathbf{r}}{2}, t\right) \\ &= Z_S^{1/2}(r) S^\dagger(\mathbf{r}, \mathbf{R}, t) \\ \hat{O}_B^{\dagger i}(\mathbf{r}, \mathbf{R}, t) &\equiv \psi^\dagger\left(\frac{\mathbf{r}}{2}, t\right) W\left(\frac{\mathbf{r}}{2}, \mathbf{R}; t\right) B^i(\mathbf{R}; t) W\left(\mathbf{R}, -\frac{\mathbf{r}}{2}; t\right) \times \\ &\times \chi\left(-\frac{\mathbf{r}}{2}, t\right) = (Z_H^{1/2})^{ij}(\mathbf{r}) H^{\dagger j}(\mathbf{r}, \mathbf{R}, t), \end{aligned} \quad (22)$$

where  $W(\mathbf{r}, \mathbf{r}'; t)$  are straight Wilson lines joining the points  $\mathbf{r}$  and  $\mathbf{r}'$  at a fixed time  $t$ , and

$$(Z_H^{1/2})^{ij}(\mathbf{r}) = Z_\Sigma^{1/2}(r) \hat{r}^i \hat{r}^j + Z_\Pi^{1/2}(r) (\delta^{ij} - \hat{r}^i \hat{r}^j). \quad (23)$$

In the static limit we have,

$$\begin{aligned} &< 0 | T \{ \hat{O}^\dagger(\mathbf{r}', \mathbf{R}', T/2) \hat{O}(\mathbf{r}, \mathbf{R}, -T/2) \} | 0 > \\ &= < 1 >_\square \delta(\mathbf{r}' - \mathbf{r}) \delta(\mathbf{R}' - \mathbf{R}) \\ &< 0 | T \{ \hat{O}_B^{\dagger i}(\mathbf{r}', \mathbf{R}', T/2) \hat{O}_B^j(\mathbf{r}, \mathbf{R}, -T/2) \} | 0 > \\ &= < B^i(\mathbf{R}', T/2) B^j(\mathbf{R}; -T/2) >_\square \delta(\mathbf{r}' - \mathbf{r}) \delta(\mathbf{R}' - \mathbf{R}), \end{aligned} \quad (24)$$

where  $< \dots >_\square$  means insertions in the square Wilson loop going from  $-T/2$  to  $T/2$  with spatial boundaries at  $\mathbf{R} \pm \mathbf{r}/2$ . In particular  $< 1 >_\square$  is the Wilson loop

itself. The matching calculation at  $\mathcal{O}(1)$  leads to,

$$\begin{aligned} < 1 >_\square &= Z_S e^{-iTV_{\Sigma_g^+}(r)} \\ < B^i(\mathbf{R}, T/2) B^j(\mathbf{R}; -T/2) >_\square \\ &= \hat{r}^i \hat{r}^j Z_\Sigma e^{-iTV_{\Sigma_u^-}(r)} + (\delta^{ij} - \hat{r}^i \hat{r}^j) Z_\Pi e^{-iTV_{\Pi_u}(r)}. \end{aligned} \quad (25)$$

Hence  $V_{\Sigma_u^-}(r)$  and  $V_{\Pi_u}(r)$  can be obtained from large  $T$  behavior of certain operator insertions in the Wilson loop, and are known since long from lattice calculations [7, 8, 23].

The NRQCD Lagrangian density at  $\mathcal{O}(1/m_Q)$  reads

$$\begin{aligned} \mathcal{L}_{NRQCD} &= \psi^\dagger \left[ iD_0 + \frac{\mathbf{D}^2}{2m_Q} + g_{c_F} \frac{\boldsymbol{\sigma} \mathbf{B}}{2m_Q} \right] \psi \\ &+ \chi^\dagger \left[ iD_0 - \frac{\mathbf{D}^2}{2m_Q} - g_{c_F} \frac{\boldsymbol{\sigma} \mathbf{B}}{2m_Q} \right] \chi, \end{aligned} \quad (26)$$

where  $c_F$  is a matching coefficient that will eventually be approximated by its tree level value  $c_F = 1$ . Since the Lagrangian above contains a spin-dependent term, we expect the leading contribution to  $V_S^{ij}$  to appear at  $\mathcal{O}(1/m_Q)$ . We can easily get it by matching the following correlation function at  $\mathcal{O}(1/m_Q)$ ,

$$\begin{aligned} &< 0 | T \{ \hat{O}(\mathbf{r}', \mathbf{R}', T/2) \hat{O}_B^{\dagger i}(\mathbf{r}, \mathbf{R}, -T/2) \} | 0 > \\ &= Z_S^{1/2} (Z_H^{1/2})^{ij}(\mathbf{r}) < 0 | T \{ S(\mathbf{r}', \mathbf{R}', T/2) H^{\dagger j}(\mathbf{r}, \mathbf{R}, -T/2) \} | 0 > \end{aligned} \quad (27)$$

and focusing on the spin-dependent terms. The lhs is calculated using first order in perturbation theory in  $1/m_Q$  in NRQCD (26). The rhs is calculated again at first order in perturbation theory in  $1/m_Q$  from (18) (recall that  $V_S^{ij}$  is treated as  $\mathcal{O}(1/m_Q)$ ). Taking into account (19), we obtain,

$$\begin{aligned} &\frac{g_{c_F}}{2m_Q} \int_{-T/2}^{T/2} dt < \hat{\mathbf{r}} \mathbf{B}(\frac{\mathbf{r}}{2}, t) \hat{\mathbf{r}} \mathbf{B}(\mathbf{0}, -T/2) >_\square \\ &< 1 >_\square^{1/2} < \hat{\mathbf{r}} \mathbf{B}(\mathbf{0}, T/2) \hat{\mathbf{r}} \mathbf{B}(\mathbf{0}, -T/2) >_\square^{1/2} \\ &= 2V_S^\Sigma \frac{\sin\left((V_{\Sigma_u^-} - V_{\Sigma_g^+})T/2\right)}{V_{\Sigma_u^-} - V_{\Sigma_g^+}} \\ &\frac{g_{c_F}}{2m_Q} \int_{-T/2}^{T/2} dt < 1 >_\square^{1/2} \times \\ &< \mathbf{B}(\frac{\mathbf{r}}{2}, t) \mathbf{B}(\mathbf{0}, -T/2) - \hat{\mathbf{r}} \mathbf{B}(\frac{\mathbf{r}}{2}, t) \hat{\mathbf{r}} \mathbf{B}(\mathbf{0}, -T/2) >_\square \\ &< \mathbf{B}(\mathbf{0}, T/2) \mathbf{B}(\mathbf{0}, -T/2) - \hat{\mathbf{r}} \mathbf{B}(\mathbf{0}, T/2) \hat{\mathbf{r}} \mathbf{B}(\mathbf{0}, -T/2) >_\square^{1/2} \\ &= 2\sqrt{2} V_S^\Pi \frac{\sin\left((V_{\Pi_u} - V_{\Sigma_g^+})T/2\right)}{V_{\Pi_u} - V_{\Sigma_g^+}}. \end{aligned} \quad (28)$$

Notice that the Euclidean version of the objects on the lhs can be easily calculated on the lattice. At large  $T$ ,  $V_S^\Sigma$  and  $V_S^\Pi$  can be then extracted by matching the data to the Euclidean version of the rhs, once  $V_{\Sigma_g^+}$ ,  $V_{\Sigma_u^-}$  and  $V_{\Pi_u}$  are known. In the following sections we are going to derive short and long distance constraints on these potentials using weak coupling pNRQCD [6, 12] and the QCD effective string theory [13, 14] respectively.



### 1. Short distance constraints

At short distances, the time evolution of a  $Q\bar{Q}$  pair is described by the weak coupling regime of pNRQCD [6, 12], the Lagrangian of which has been displayed in (15) at next-to-leading order in the multipole expansion. The operators  $\hat{O}(\mathbf{r}, \mathbf{R}, t)$  and  $\hat{O}_B^i(\mathbf{r}, \mathbf{R}, t)$  match onto the singlet field  $S(\mathbf{r}, \mathbf{R}, t)$  and the operator  $\text{tr}(O(\mathbf{r}, \mathbf{R}, t)B^i(\mathbf{R}, t))$  respectively. The leading spin-dependent term in the pNRQCD Lagrangian reads [24],

$$\mathcal{L}'_{pNRQCD} = \frac{g_{CF}}{2m_Q} \text{Tr} \left( O^\dagger(\mathbf{r}, \mathbf{R}, t) \mathbf{B}(\mathbf{R}, t) \{ \boldsymbol{\sigma}, S(\mathbf{r}, \mathbf{R}, t) \} \right) + \text{H.c.} \quad (30)$$

We use  $\text{tr}$  for trace over color indices and  $\text{Tr}$  for trace over both color and spin indices. Notice that the term above shows an  $\mathbf{r}$ -independent interaction between the singlet field and the operator  $\text{tr}(OB^i)$ , which implies that

$$V_S^\Sigma(r) = V_S^\Pi(r) = \pm \frac{c_F \lambda^2}{m_Q}, \quad (31)$$

where  $\lambda \sim \Lambda_{\text{QCD}}$  is a constant, and we have put the sign explicitly.

### 2. Long distance constraints

At long distances the energy spectrum of a static  $Q\bar{Q}$  pair is well described by the QCD effective string theory (EST) [13, 14]. The mapping between operator insertions in the temporal Wilson lines of the Wilson loop and the corresponding operators in the EST was established in [25], following earlier work [26]. For the relevant operators to us, it reads,

$$\begin{aligned} B^l(t, \mathbf{r}/2) &\rightarrow \Lambda' \epsilon^{lm} \partial_t \partial_z \xi^m(t, r/2) \\ B^l(t, -\mathbf{r}/2) &\rightarrow \Lambda' \epsilon^{lm} \partial_t \partial_z \xi^m(t, -r/2) \\ B^3(t, \mathbf{r}/2) &\rightarrow \Lambda''' \epsilon^{lm} \partial_t \partial_z \xi^l(t, r/2) \partial_z \xi^m(t, r/2) \\ B^3(t, -\mathbf{r}/2) &\rightarrow \Lambda''' \epsilon^{lm} \partial_t \partial_z \xi^l(t, -r/2) \partial_z \xi^m(t, -r/2), \end{aligned} \quad (32)$$

where  $l, m = 1, 2$ . Here, we also need to map the states created by operator insertions in spacial Wilson lines to the corresponding states in EST. In order to do so it is convenient to take the  $\mathbf{r}$  along the  $z$  axis, and write the EST Lagrangian in terms of the complex field  $\varphi(z, t) = (\xi^1(z, t) + i\xi^2(z, t))/\sqrt{2}$ . This field has nice transformation properties under  $D_{\infty h}$ , the relevant space group,

$$\begin{aligned} R_z(\theta): \varphi(z, t) &\rightarrow e^{i\theta} \varphi(z, t) \\ P : \varphi(z, t) &\rightarrow -\varphi(-z, t) \\ R_{xz} : \varphi(z, t) &\rightarrow \varphi^*(z, t), \end{aligned} \quad (33)$$

where  $R_z(\theta)$ ,  $P$  and  $R_{xz}$  stand for a rotation of angle  $\theta$  around the  $z$  axis, a parity transformation, and a reflexion through the  $xz$  plain respectively. The Lagrangian density at LO reads,

$$\mathcal{L}_{EST} = \kappa \partial_\mu \varphi \partial^\mu \varphi^*, \quad (34)$$

where  $\kappa$  is the string tension and  $\varphi(z, t)$  fulfils Dirichlet boundary conditions,  $\varphi(r/2, t) = \varphi(-r/2, t) = 0$ .  $\varphi(z, t)$  can be written in terms of creation and annihilation operators

$$\begin{aligned} \varphi(z, t) &= \sum_{n=1}^{\infty} \frac{1}{2E_n} (e^{-iE_n t} \varphi_n(z) a_n + e^{iE_n t} \varphi_n^*(z) b_n^\dagger) \\ \varphi_n(z) &= \frac{1}{\sqrt{2r}} (e^{iE_n z} + (-1)^{n+1} e^{-iE_n z}) \end{aligned} \quad (35)$$

$$[a_n, a_m^\dagger] = [b_n, b_m^\dagger] = \frac{2E_n}{\kappa} \delta_{nm}, \quad E_n = \frac{\pi n}{r}.$$

The remaining commutators vanish.  $a_n^\dagger$  ( $b_n^\dagger$ ) on the vacuum creates a state of energy  $E_n$ , angular momentum 1 ( $-1$ ) and parity  $(-1)^n$ . The reflexion with respect to the  $xz$  plain interchanges  $a_n \leftrightarrow b_n$ . If we define

$$\begin{aligned} \hat{O}_B^\dagger(\mathbf{r}, \mathbf{0}, t) &= \hat{O}_B^\dagger(\mathbf{r}, \mathbf{0}, t) + i\hat{O}_B^{\dagger 2}(\mathbf{r}, \mathbf{0}, t) \\ \hat{O}_B^{\dagger*}(\mathbf{r}, \mathbf{0}, t) &= \hat{O}_B^\dagger(\mathbf{r}, \mathbf{0}, t) - i\hat{O}_B^{\dagger 2}(\mathbf{r}, \mathbf{0}, t), \end{aligned} \quad (36)$$

then the following identifications fulfil the  $D_{\infty h}$  symmetry requirements,

$$\begin{aligned} \hat{O}^\dagger(\mathbf{r}, \mathbf{0}, -T/2)|0\rangle &\rightarrow |0\rangle \\ \hat{O}_B^{\dagger 3}(\mathbf{r}, \mathbf{0}, -T/2)|0\rangle &\rightarrow \frac{\kappa}{2\sqrt{2E_1 E_2}} (a_1^\dagger b_2^\dagger - b_1^\dagger a_2^\dagger) |0\rangle \\ \hat{O}_B^\dagger(\mathbf{r}, \mathbf{0}, -T/2)|0\rangle &\rightarrow \sqrt{\frac{\kappa}{2E_1}} b_1^\dagger |0\rangle \\ \hat{O}_B^{\dagger*}(\mathbf{r}, \mathbf{0}, -T/2)|0\rangle &\rightarrow -\sqrt{\frac{\kappa}{2E_1}} a_1^\dagger |0\rangle. \end{aligned} \quad (37)$$

Let us perform analogous definitions for the chromomagnetic fields,

$$\begin{aligned} B(t, \mathbf{r}) &= B^1(t, \mathbf{r}) + iB^2(t, \mathbf{r}) \\ B^*(t, \mathbf{r}) &= B^1(t, \mathbf{r}) - iB^2(t, \mathbf{r}). \end{aligned} \quad (38)$$

The mapping (32) then reads,

$$\begin{aligned} B(t, \pm\mathbf{r}/2) &\rightarrow -i\sqrt{2}\Lambda' \partial_t \partial_z \varphi(\pm r/2, t) \\ B^*(t, \pm\mathbf{r}/2) &\rightarrow i\sqrt{2}\Lambda' \partial_t \partial_z \varphi^*(\pm r/2, t) \\ B^3(t, \pm\mathbf{r}/2) &\rightarrow i\Lambda''' \partial_t \partial_z \varphi(\pm r/2, t) \partial_z \varphi^*(\pm r/2, t) + \text{H.c.} \end{aligned} \quad (39)$$

Upon substituting the above expressions and (37) in (28), we obtain,

$$V_S^\Sigma(r) = -\frac{\pi^2 g \Lambda''' c_F}{m_Q \kappa r^3}, \quad V_S^\Pi(r) = \frac{\pi^{3/2} g \Lambda' c_F}{2m_Q \sqrt{\kappa} r^2}. \quad (40)$$

The parameters  $g\Lambda' \sim \Lambda_{\text{QCD}}$  and  $g\Lambda''' \sim \Lambda_{\text{QCD}}$  also appear in the spin-orbit and tensor potentials of heavy

quarkonium [25, 27], which have been calculated on the lattice [23, 29]. We obtain from fits to the data of ref. [28],

$$g\Lambda' \sim -59\text{MeV} \quad , \quad g\Lambda''' \sim \pm 230\text{MeV} \quad , \quad (41)$$

Details on the fits are given in the Appendix B<sup>2</sup>.

### 3. Modeling the mixing potential

For the actual mixing potentials we use a simple interpolation between (31) and (40) that allows for a sign flip between the short and long distance expressions without introducing any further scale, namely,

$$V_S^\Pi[\pm-](r) = \frac{\lambda^2}{m_Q} \left( \frac{\pm 1 - (\frac{r}{r_\Pi})^2}{1 + (\frac{r}{r_\Pi})^4} \right) \quad (42)$$

$$V_S^\Sigma[\pm\pm](r) = \frac{\lambda^2}{m_Q} \left( \frac{\pm 1 \pm (\frac{r}{r_\Sigma})^2}{1 + (\frac{r}{r_\Sigma})^5} \right) \quad , \quad (43)$$

where  $r_\Pi = (\frac{|g\Lambda'| \pi^{\frac{3}{2}}}{2\lambda^2 \kappa^{\frac{1}{2}}})^{\frac{1}{2}}$  and  $r_\Sigma = (\frac{|g\Lambda'''| \pi^2}{\lambda^2 \kappa})^{\frac{1}{3}}$ . Note that the  $\pm$  in  $V_S^\Pi$  and the first  $\pm$  in  $V_S^\Sigma$  are correlated because both potentials have the same short distance behavior. We will explore the following values for the only unknown parameter  $\lambda$ ,  $\lambda = 100, 300, 600$  MeV, and all possible sign combinations for the  $1^{--}$  charmonium states below, and choose the one that suits better the phenomenology.

## B. Mixing equations

Now, we need to include the quark spin degree of freedom to the equations displayed in section II. Let us write,

$$S = \frac{1}{\sqrt{2}} (S_0 + \sigma^k S_1^k) \quad (44)$$

$$H^j = \frac{1}{\sqrt{2}} (H_0^j + \sigma^i H_1^{ji}) \quad ,$$

where we have omitted the arguments in  $S = S(\mathbf{R}, \mathbf{r}, t)$  and  $H^j = H^j(\mathbf{R}, \mathbf{r}, t)$ , the subscript 0, 1 stands for the total spin of the quark-antiquark pair, and the superscripts  $k, i$  label the three states in the spin 1 case. Recall that the superscript  $j$  labels the three states of the total angular momentum 1 of the gluonic degrees of freedom. Then the last term in (18) reads,

$$\text{tr} \left( S^\dagger V_S^{ij} \{ \sigma^i, H^j \} \right) = 2V_S^{ij} \left( S_1^{i\dagger} H_0^j + S_0^\dagger H_1^{ji} \right) \quad . \quad (45)$$

<sup>2</sup> Due to an error in the identification, the value of  $g\Lambda'$  displayed in [11] as  $\Lambda'$  is twice the actual value. This change does not affect the statements made in that paper.

Note that this term mixes spin 0 (1) hybrids with spin 1 (0) quarkonium. In view of the decomposition of  $V_S^{ij}$  in (19), we only need to analyze  $S_1^{j\dagger} H_0^j$ ,  $S_1^{i\dagger} H_0^j \hat{r}^i \hat{r}^j$ ,  $S_0^\dagger H_1^{jj}$  and  $S_0^\dagger H_1^{ji} \hat{r}^i \hat{r}^j$ . Consider the first expression,

$$\int d\Omega S_1^{j\dagger} H_0^j = \sum_{JML} \frac{S_{1JM}^{L\dagger} P_{0JM}^L}{r^2} = \sum_{JML} \frac{S_{1JM}^{L\dagger} P_{0JM}^L}{r^2} \quad , \quad (46)$$

where  $J$  is the orbital angular momentum, plus the quark spin for  $S_1$  and plus the gluonic total angular momentum for  $H_0$ , and  $M$  its third component.  $J = \mathcal{J}$  and  $M = \mathcal{M}$ , the total angular momentum and its third component respectively.  $L = J, J \pm 1$  are simply denoted by  $0, \pm$ . We have used above the same decomposition for  $S_1^j$  as the one used for  $H^j$  in (4). For the second expression we have,

$$\int d\Omega S_1^{i\dagger} H_0^j \hat{r}^i \hat{r}^j = \quad (47)$$

$$\frac{1}{r^2} S_{1JM}^{+\dagger} \left( \frac{\mathcal{J}}{2\mathcal{J}+1} P_{0JM}^- - \frac{\sqrt{\mathcal{J}(\mathcal{J}+1)}}{2\mathcal{J}+1} P_{0JM}^+ \right)$$

$$+ \frac{1}{r^2} S_{1JM}^{+\dagger} \left( \frac{\mathcal{J}+1}{2\mathcal{J}+1} P_{0JM}^+ - \frac{\sqrt{\mathcal{J}(\mathcal{J}+1)}}{2\mathcal{J}+1} P_{0JM}^- \right) \quad .$$

For the third and fourth expressions, we need to introduce tensor spherical harmonics  $Y_{\mathcal{J}\mathcal{M}}^{jLJ}(\hat{\mathbf{r}})$  (see appendix C), which are eigenfunctions of  $\mathbf{S}^2$ ,  $\mathbf{L}_g^2$ ,  $\mathbf{L}^2$ ,  $\mathbf{J}^2$ ,  $\mathcal{J}^2$  and  $\mathcal{J}_3$  with eigenvalue 2, 2,  $L(L+1)$ ,  $J(J+1)$ ,  $\mathcal{J}(\mathcal{J}+1)$  and  $\mathcal{M}$  respectively, with  $L = J, J \pm 1$ ,  $J = \mathcal{J}, \mathcal{J} \pm 1$ . We then have,

$$H_1^{ji}(\mathbf{r}, t) = \frac{1}{r} \sum_{LJ\mathcal{J}\mathcal{M}} Y_{\mathcal{J}\mathcal{M}}^{jiLJ}(\hat{\mathbf{r}}) P_{1\mathcal{J}\mathcal{M}}^{LJ}(r) \quad . \quad (48)$$

We will use  $0, \pm$  both for  $L = J, J \pm 1$  and  $J = \mathcal{J}, \mathcal{J} \pm 1$ . Hence,

$$\int d\Omega S_0^\dagger H_1^{jj} = \frac{1}{r^2} \sum_{\mathcal{J}\mathcal{M}} S_{0\mathcal{J}\mathcal{M}}^+ \times \quad (49)$$

$$\left( -\sqrt{\frac{2\mathcal{J}-1}{2\mathcal{J}+1}} P_{1\mathcal{J}\mathcal{M}}^{+-} + P_{1\mathcal{J}\mathcal{M}}^{00} - \sqrt{\frac{2\mathcal{J}+3}{2\mathcal{J}+1}} P_{1\mathcal{J}\mathcal{M}}^{-+} \right)$$

$$\int d\Omega S_0^\dagger H_1^{ji} \hat{r}^i \hat{r}^j = \frac{1}{r^2} \sum_{\mathcal{J}\mathcal{M}} S_{0\mathcal{J}\mathcal{M}}^+ \times \quad (50)$$

$$\left( \sqrt{\frac{\mathcal{J}(\mathcal{J}-1)}{(2\mathcal{J}+1)(2\mathcal{J}-1)}} P_{1\mathcal{J}\mathcal{M}}^{--} - \frac{\mathcal{J}}{\sqrt{(2\mathcal{J}+3)(2\mathcal{J}+1)}} P_{1\mathcal{J}\mathcal{M}}^{+-} + \right.$$

$$\left. + \sqrt{\frac{(\mathcal{J}+1)(\mathcal{J}+2)}{(2\mathcal{J}+1)(2\mathcal{J}+3)}} P_{1\mathcal{J}\mathcal{M}}^{++} - \frac{\mathcal{J}+1}{\sqrt{(2\mathcal{J}+3)(2\mathcal{J}+1)}} P_{1\mathcal{J}\mathcal{M}}^{-+} \right) \quad .$$

Putting all together, we get the following sets of coupled equations. For  $S = 0$  hybrids, we have for

$\mathcal{J} \neq 0$

$$\left[ -\frac{1}{m_Q} \frac{\partial^2}{\partial r^2} + \frac{\mathcal{J}(\mathcal{J}+1)}{m_Q r^2} + \begin{pmatrix} V_{\Sigma_g^+} & 2V_S^\Pi \\ 2V_S^\Pi & V_{\Pi_u} \end{pmatrix} \right] \begin{pmatrix} S_{1\mathcal{J}\mathcal{M}}^0(r) \\ P_{0\mathcal{J}\mathcal{M}}^0(r) \end{pmatrix} = E \begin{pmatrix} S_{1\mathcal{J}\mathcal{M}}^0(r) \\ P_{0\mathcal{J}\mathcal{M}}^0(r) \end{pmatrix}. \quad (51)$$

$$\left[ -\frac{1}{m_Q} \frac{\partial^2}{\partial r^2} + \begin{pmatrix} \frac{(\mathcal{J}+1)(\mathcal{J}+2)}{m_Q r^2} + V_{\Sigma_g^+} & 0 & 2(V_S^\Pi + \frac{\mathcal{J}+1}{2\mathcal{J}+1} V_S^q) & -2V_S^q \frac{\sqrt{\mathcal{J}(\mathcal{J}+1)}}{2\mathcal{J}+1} \\ 0 & \frac{(\mathcal{J}-1)\mathcal{J}}{m_Q r^2} + V_{\Sigma_g^+} & -2V_S^q \frac{\sqrt{\mathcal{J}(\mathcal{J}+1)}}{2\mathcal{J}+1} & 2(V_S^\Pi + \frac{\mathcal{J}}{2\mathcal{J}+1} V_S^q) \\ 2(V_S^\Pi + \frac{\mathcal{J}+1}{2\mathcal{J}+1} V_S^q) & -2\frac{\sqrt{\mathcal{J}(\mathcal{J}+1)}}{2\mathcal{J}+1} & \frac{(\mathcal{J}+1)(\mathcal{J}+2)}{m_Q r^2} + V_{\Sigma_u^-} + \frac{\mathcal{J}}{2\mathcal{J}+1} V_q & \frac{\sqrt{\mathcal{J}(\mathcal{J}+1)}}{2\mathcal{J}+1} V_q \\ -2V_S^q \frac{\sqrt{\mathcal{J}(\mathcal{J}+1)}}{2\mathcal{J}+1} & 2(V_S^\Pi + \frac{\mathcal{J}}{2\mathcal{J}+1} V_S^q) & \frac{\sqrt{\mathcal{J}(\mathcal{J}+1)}}{2\mathcal{J}+1} V_q & \frac{(\mathcal{J}-1)\mathcal{J}}{m_Q r^2} + V_{\Sigma_u^-} + \frac{\mathcal{J}+1}{2\mathcal{J}+1} V_q \end{pmatrix} - E \right] \begin{pmatrix} S_{1\mathcal{J}\mathcal{M}}^+(r) \\ S_{1\mathcal{J}\mathcal{M}}^-(r) \\ P_{0\mathcal{J}\mathcal{M}}^+(r) \\ P_{0\mathcal{J}\mathcal{M}}^-(r) \end{pmatrix} = 0, \quad (52)$$

where  $V_S^q = V_S^\Sigma - V_S^\Pi$ . For  $\mathcal{J} = 0$ , equations (51) do not exist and equations (52) reduce to two coupled equations for  $S_{100}^+(r)$  and  $P_{000}^+(r)$ . For  $S = 1$  hybrids,  $P_{1\mathcal{J}\mathcal{M}}^{+0}(r)$  and  $P_{1\mathcal{J}\mathcal{M}}^{-0}(r)$  do not couple to heavy quarkonium. The remaining do it according to the following equations for  $\mathcal{J} > 1$ ,

$$\left[ \frac{1}{m_Q} \frac{\partial^2}{\partial r^2} - \begin{pmatrix} \frac{\mathcal{J}(\mathcal{J}+1)}{m_Q r^2} + V_{\Sigma_g^+} & V_S^{++} & V_S^{-+} & V_S^{+-} & V_S^{--} & V_S^\Pi \\ V_S^{++} & \frac{(\mathcal{J}+2)(\mathcal{J}+3)}{m_Q r^2} + V^{++} & -2V_q \frac{\sqrt{(\mathcal{J}+1)(\mathcal{J}+2)}}{2\mathcal{J}+3} & 0 & 0 & 0 \\ V_S^{-+} & -2V_q \frac{\sqrt{(\mathcal{J}+1)(\mathcal{J}+2)}}{2\mathcal{J}+3} & \frac{\mathcal{J}(\mathcal{J}+1)}{m_Q r^2} + V^{-+} & 0 & 0 & 0 \\ V_S^{+-} & 0 & 0 & \frac{\mathcal{J}(\mathcal{J}+1)}{m_Q r^2} + V^{+-} & V_q \frac{\sqrt{(\mathcal{J}-1)\mathcal{J}}}{2\mathcal{J}-1} & 0 \\ V_S^{--} & 0 & 0 & V_q \frac{\sqrt{(\mathcal{J}-1)\mathcal{J}}}{2\mathcal{J}-1} & \frac{(\mathcal{J}-1)\mathcal{J}}{m_Q r^2} + V^{--} & 0 \\ V_S^\Pi & 0 & 0 & 0 & 0 & \frac{\mathcal{J}(\mathcal{J}+1)}{m_Q r^2} + V_{\Pi_u} \end{pmatrix} + E \right] \begin{pmatrix} S_{0\mathcal{J}\mathcal{M}}(r) \\ P_{1\mathcal{J}\mathcal{M}}^{++}(r) \\ P_{1\mathcal{J}\mathcal{M}}^{+-}(r) \\ P_{1\mathcal{J}\mathcal{M}}^{--}(r) \\ P_{1\mathcal{J}\mathcal{M}}^{00}(r) \end{pmatrix} = 0, \quad (53)$$

where,

$$\begin{aligned} V_S^{++} &= \sqrt{\frac{(\mathcal{J}+1)(\mathcal{J}+2)}{(2\mathcal{J}+1)(2\mathcal{J}+3)}} V_S^q \\ V_S^{-+} &= -\frac{\mathcal{J}+1}{\sqrt{(2\mathcal{J}+3)(2\mathcal{J}+1)}} V_S^q - \sqrt{\frac{2\mathcal{J}+3}{2\mathcal{J}+1}} V_S^\Pi \\ V_S^{+-} &= -\frac{\mathcal{J}}{\sqrt{(2\mathcal{J}+3)(2\mathcal{J}-1)}} V_S^q - \\ &\quad -V_S^\Pi \frac{\sqrt{(2\mathcal{J}-1)(2\mathcal{J}+1)}}{2\mathcal{J}+1} \end{aligned}$$

$$\begin{aligned} V_S^{--} &= \sqrt{\frac{\mathcal{J}(\mathcal{J}-1)}{(2\mathcal{J}+1)(2\mathcal{J}-1)}} V_S^q \\ V^{++} &= V_{\Sigma_u^-} + \frac{\mathcal{J}+1}{2\mathcal{J}+3} V_q \\ V^{-+} &= V_{\Sigma_u^-} + \frac{\mathcal{J}+2}{2\mathcal{J}+3} V_q \\ V^{+-} &= V_{\Sigma_u^-} + \frac{\mathcal{J}-1}{2\mathcal{J}-1} V_q \\ V^{--} &= V_{\Sigma_u^-} + \frac{\mathcal{J}}{2\mathcal{J}-1} V_q. \end{aligned} \quad (54)$$

For  $\mathcal{J} = 0$ ,  $P_{100}^{00}(r)$ ,  $P_{100}^{--}(r)$  and  $P_{100}^{+-}(r)$  do not exist, and the system reduces to the three upper equations.  $P_{100}^{0-}(r)$ , which does not couple to heavy quarkonium, does not exist either. For  $\mathcal{J} = 1$ ,  $P_{11\mathcal{M}}^{--}(r)$  does not exist and the system above reduces to five coupled equations.

### C. Spectrum

In order to fix the signs and the parameter  $\lambda$  of the mixing potentials, we focus on the spin zero  $n(s/d)_1$  ( $n = 1, 2, 3$ ), states in table I, which can be identified with  $Y(4008)$ ,  $Y(4360)$  and  $Y(4660)$ . The main problem with this identification is that all three states have been observed to decay to spin one quarkonium states, which violates spin symmetry. However, according to eq. (52) the spin zero hybrids mix with spin one quarkonium, and hence, if this mixing is large, we may find a natural explanation to these decays. We present our results in table IV (the case  $\lambda = 100$  MeV is not displayed, it produces a tiny mixing in all cases). We observed that the case that provides the largest amount of mixing is the combination  $V_S^\Pi[+-]$  with

$V_S^\Sigma[++]$  and  $\lambda = 600$  MeV. This is the sign combination and the value of  $\lambda$  that we will take for the rest of the paper. The spectrum of charmonium and charmonium hybrids is given in tables IV-XII and the one of bottomonium and bottomonium hybrids in tables XIII-XX. The general trend (with a few exceptions) is that hybrid states get heavier whereas quarkonium states get lighter due the mixing.

Since we have used leading order potential for both quarkonium and hybrids, the potentials we missed start at order  $1/m_Q$ . Hence the error to assign to

this calculation for the hybrids is  $\Lambda_{\text{QCD}}^2/m_Q$ , since  $\Lambda_{\text{QCD}}$  is the next relevant scale. For quarkonium this is not always the case, since the typical momenta can be larger than  $\Lambda_{\text{QCD}}$ . A detailed error analysis is carried out in the Appendix A. For simplicity, we will stick to the  $\Lambda_{\text{QCD}}^2/m_Q$  estimate for quarkonium as well. Taking  $\Lambda_{\text{QCD}} \sim 400$  MeV, we obtain a precision of about 110 MeV for charmonium, and 33 MeV for bottomonium. These are the numbers we will have in mind when comparing to experiment and to other approaches.

$NL_J$	$\lambda = 0$	%	$V_S^\Pi[+-], V_S^\Sigma[++]$				$V_S^\Pi[+-], V_S^\Sigma[+-]$				$V_S^\Pi[--], V_S^\Sigma[-+]$				$V_S^\Pi[--], V_S^\Sigma[--]$			
			$\lambda = 0.3$	%	$\lambda = 0.6$	%	$\lambda = 0.3$	%	$\lambda = 0.6$	%	$\lambda = 0.3$	%	$\lambda = 0.6$	%	$\lambda = 0.3$	%	$\lambda = 0.6$	%
1s	3.068	0	3.064	0	3.001	4	3.066	0	3.053	0	3.063	0	3.036	2	3.061	1	2.989	6
2s	3.678	0	3.672	1	3.628	14	3.677	1	3.670	4	3.677	0	3.661	4	3.672	1	3.630	7
1d	3.793	0	3.773	4	3.687	12	3.790	1	3.785	2	3.792	0	3.789	0	3.782	1	3.712	7
1(s/d) <sub>1</sub>	4.011	100	4.016	96	4.014	71	4.012	99	4.004	96	4.014	99	4.025	99	4.016	98	4.040	85
3s	4.131	0	4.127	0	4.107	10	4.128	1	4.130	7	4.130	0	4.125	10	4.128	2	4.103	12
2d	4.210	0	4.203	20	4.180	79	4.209	10	4.207	39	4.209	2	4.205	5	4.204	1	4.172	52
2(s/d) <sub>1</sub>	4.355	100	4.358	97	4.366	65	4.356	98	4.355	89	4.357	100	4.368	94	4.357	100	4.383	86
4s	4.512	0	4.515	0	4.497	0	4.517	1	4.513	7	4.517	0	4.508	8	4.515	1	4.495	0
3d	4.579	0	4.573	2	4.559	8	4.578	0	4.574	5	4.578	1	4.568	7	4.574	0	4.550	3
3(s/d) <sub>1</sub>	4.692	100	4.699	98	4.711	83	4.694	99	4.699	93	4.693	100	4.699	97	4.698	99	4.724	90
4(s/d) <sub>1</sub>	4.718	100	4.730	100	4.785	96	4.719	100	4.718	98	4.720	100	4.728	98	4.728	100	4.779	97
5s	4.865	0	4.864	0	4.848	3	4.865	0	4.865	7	4.865	0	4.867	7	4.864	1	4.846	2
4d	4.916	0	4.913	7	4.903	35	4.915	2	4.915	19	4.915	0	4.912	12	4.913	3	4.894	21
5(s/d) <sub>1</sub>	5.043	100	5.044	99	5.046	84	5.043	99	5.043	94	5.044	100	5.050	97	5.044	100	5.067	93

TABLE IV. Spectrum of charmonium ( $S = 1$ ) and charmonium hybrids ( $S = 0$ ):  $1^{--}$  states. Masses are in GeV. The % columns show the fraction of the hybrid components for the mass states in the previous column.  $m_c = 1.47$  GeV.

## V. COMPARISON WITH OTHER APPROACHES

In this section, we compare our results with other QCD based approaches. For convenience we will compare our results for the spectrum in the case  $\lambda = 0$  (no mixing). The shifts in the spectrum due to mixing are within our estimated errors.

### A. Born-Oppenheimer approximation

In [4], the lower lying bottomonium hybrid spectrum was calculated from the static potentials  $\Pi_u$  and  $\Sigma_u^-$  and normalized to the bottomonium spectrum. The mixing between hybrid states built out of these potentials that appears at leading order due to the kinetic term of the heavy quarks was ignored. The masses obtained for  $H_1$  ( $1(s/d)_1$ ),  $H_2$  ( $1p_1$ ),  $H_3$  ( $1p_0$ ), and  $H'_1$  ( $2(s/d)_1$ ) are between 150-300 MeV heavier

than ours. This is probably due to the different choice of the bottom quark mass.

In [9], the lower lying hybrid spectrum was calculated as above. However, for charmonium, the ground state for each potential was fixed to the lattice data of ref. [30]. The mixing between hybrid states was also ignored. If we compare the splittings obtained from table X of [9] with those obtained from our tables I and II, we find agreement within 20 MeV, except for the  $H_4$ - $H_1$  case for which we obtain a lower value by about 40 MeV and the  $H'_3$  -  $H_3$  case for which we obtain a higher value of about 70 MeV. We have identified the states  $H_1$ ,  $H'_1$ ,  $H_2$ ,  $H'_2$ ,  $H''_2$ ,  $H_3(1P)$  and  $H_4$  with  $1(s/d)_1$ ,  $2(s/d)_1$ ,  $1p_1$ ,  $1d_2$ ,  $2p_1$ ,  $3(s/d)_1$  and  $1(p/f)_2$  respectively.

Our hybrid spectrum is compatible within errors with that of ref. [10] both for charmonium and bottomonium, except for the bottomonium  $1(s/d)_1$  and  $2p_0$  states, for which we have slightly lower masses. Our central values tend to be at the lower end of their

error bars. Although the construction of the effective theory for hybrids is somewhat different and the parametrization of the potentials as well, the most relevant difference is probably the normalization of the spectrum. Indeed, in ref. [10] the hybrid spectrum is normalized using the charm and bottom masses in the RS scheme [31], whereas here we normalize it to the corresponding quarkonium spectrum, which is not calculated in that reference. We have checked that we reproduce the results of ref. [10] with our code if we input their potentials<sup>3</sup>.

## B. Lattice QCD

In [32], the spectrum of the lightest exotic charmonium hybrids is calculated in the quenched approximation for a relativistic charm action in an anisotropic lattice ( $a_s = 0.197 - 0.09$  fm,  $a_s/a_t=2$ ). Their results for the  $1^{-+}$ ,  $0^{+-}$  and  $2^{+-}$  states are between 400–700 MeV higher than ours.

There has been a recent update [33] of earlier results [30] by the Hadronic Spectrum Collaboration for the charmonium spectrum including hybrid states. They use relativistic charm and dynamical light quarks in an anisotropic lattice with temporal spacing  $a_t \sim 0.034$  fm and spatial spacing  $a_s \sim 0.12$  fm. The update basically consists of taking up and down quark masses smaller than in the previous calculation ( $m_\pi \sim 240$  MeV and  $m_\pi \sim 400$  MeV respectively). The hierarchy of the lowest lying hybrid multiplets agrees with ours, from lighter to heavier:  $1(s/d)_1$ ,  $1p_1$ ,  $1(p/f)_2$  and  $1p_0$ . However, their numbers are considerable larger than ours: 381 MeV, 326 MeV, 392 MeV and 151 MeV higher for the spin average of the  $1(s/d)_1$ ,  $1p_1$ ,  $1(p/f)_2$  and  $1p_0$  multiplets respectively. The hierarchy in which quarkonium and hybrid states arise agrees for the  $1^{++}$  (4 states) and  $1^{+-}$  (6 states) quantum numbers but disagrees for the remaining non-exotic ones.

In [34], the lower lying charmonium spectrum is also calculated with four dynamical quarks in a Wilson twisted mass action. Lattice spacings ranging from 0.0619 fm to 0.0885 fm and pion masses ranging from 225 MeV to 470 MeV are used and both the continuum and the chiral extrapolations are carried out. They find a  $1^{--}$  state at 3951 MeV that is compatible with our  $1(s/d)_1$  spin zero hybrid state (4011 MeV). With less significance, they also find two  $2^{++}$  states at about 4460 MeV and 4530 MeV which are compatible with our  $2f$  quarkonium (4428 MeV) and  $2(p/f)_2$  spin zero hybrid (4563 MeV) respectively.

In [4], the bottomonium hybrid spectrum is calculated in quenched lattice NRQCD using an anisotropic lattice ( $a_s \sim 0.11$  fm,  $a_s/a_t = 3$ ). They find the lightest hybrid  $H_1$  ( $1(s/d)_1$ ) 1.49(2)(5) GeV above the  $1S$  quarkonium, this is about 250 MeV heavier than ours. About the same difference is also found for  $H_2$  ( $1p_1$ ) and  $H_3$  ( $1p_0$ ), whereas for  $H'_1$  ( $2(s/d)_1$ ) the difference raises to 470 MeV.

For bottomonium, there is also a quenched lattice calculation with relativistic bottom quarks in an anisotropic lattice ( $a_s \sim 0.04 - 0.17$  fm,  $a_s/a_t = 4, 5$ ) [35]. The masses for the lightest  $2^{--}$ ,  $1^{-+}$  and  $2^{+-}$  hybrids are displayed, which turn out to be either lighter ( $2^{--}$ ) or heavier ( $1^{-+}$  and  $2^{+-}$ ) than our results, in spite of the large errors (200 – 600 MeV).

## C. QCD sum rules

In [36], the hybrid spectrum for charmonium and bottomonium is calculated.

For charmonium, the quantum numbers of their lightest hybrid multiplet coincide with ours ( $1(s/d)_1$ ) and the masses are compatible with ours for the  $1^{-+}$  and  $2^{-+}$  states within errors (between 150 MeV and 230 MeV), but below for the  $0^{-+}$  and  $1^{--}$  states. For spin zero hybrids, they obtain a  $2^{++}$  state ( $1(p/f)_2$ ) as the second lighter state whereas we have a  $1^{++}$  state ( $1p_1$ ). The mass of the  $2^{++}$  state is, nevertheless, compatible with ours within the large errors, but the masses of the  $1^{++}$  and  $0^{++}$  states are higher. The masses of the spin one hybrids  $0^{+-}$  and  $1^{+-}$  are compatible, again within large errors.

For bottomonium, they obtain the same hierarchy of multiplets as in charmonium. However, the larger errors make it now compatible with ours, even though the central values are not. The masses of the lightest multiplet are considerably lower than ours, but the ones of the remaining multiplets ( $1^{++}$ ,  $0^{+-}$ ,  $1^{+-}$ ;  $2^{++}$ ;  $0^{++}$ ) are compatible within large errors.

## VI. COMPARISON WITH EXPERIMENT

In this section, we compare experimental results with ours in the case of maximum mixing. That is with the results displayed on the 6th column of Table IV and on the 4th column of Tables VI-XX. As mentioned before, the shifts in the spectrum due to mixing are not very important. However, the violations of heavy quark spin symmetry induced by the mixing are crucial to map our results to the XYZ states. We omit in the analysis the neutral states that have been identified as isospin partners of charged states.

<sup>3</sup> We have also checked that our results are reproduced by the code of ref. [10] if our potentials are input. We thank the authors of that reference for providing their code for the test.

### A. Charm

- $X(3823)$  [37] is compatible with our  $2^{--}$  charmonium  $1d$  state (3792 MeV).
- $X(3872)$  [37] is compatible with our  $1^{++}$  charmonium  $2p$  states (3967 MeV). Since it sits at the  $D^0\bar{D}^{0*}$  threshold, it is expected to have a large mixing with those states that we have not taken into account.
- $X(3915)$  and  $X(3940)$  [37] are also compatible with our charmonium  $2p$  states (3968 MeV). Since they are close to the  $D_s\bar{D}_s$  threshold (3936 MeV), the  $0^+$  states may have a large mixing with those states.
- $Y(4008)$  [38] is compatible with our  $1^{--}$  hybrid  $1(s/d)_1$  ( $H_1$ ) state (4004 MeV). It mixes with spin one charmonium (see column 7 in table IV and fig. 6), which may explain the observed spin symmetry violating decays.

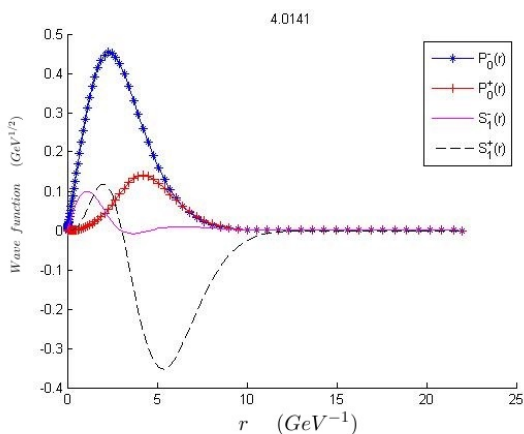


FIG. 6. The wave function of the charmonium  $1^{--} 1(s/d)_1$  state.

- $X(4140)$  [39] and  $X(4160)$  [37] are compatible with our  $1^{++}$  hybrid  $1p_1$  ( $H_2$ ) state (4146 MeV). Since the quantum numbers of  $X(4160)$  have not been established, it may also correspond to the  $1(p/f)_2$  hybrid or to the scalar  $3s$  or  $2d$  states. The fact that no decays to charmonium of the  $1p_1$  state are allowed at leading order is consistent with the fact that no such decays have been observed so far for  $X(4160)$ , which selects it as our favorite hybrid candidate for that state. If so there is no room for the  $X(4140)$  ( $1^{++}$ ) in our spectrum. These states may be affected by the  $D_s^*\bar{D}_s$  threshold (4080 MeV).
- $X(4230)$  and  $Y(4260)$  [37] are compatible with our  $1^{--}$  charmonium  $2d$  state (4180 MeV). It

may have a dominant spin zero hybrid component (see table IV), which may help to understand the recent results by the BESIII collaboration [40]. Indeed, in [41] it is claimed that the former  $Y(4260)$  peak observed in  $\pi^+\pi^-J/\psi$  invariant mass actually consists of two resonances  $Y(4220)$  and  $Y(4390)$ . The parameters of the first resonance are compatible with the ones of  $X(4230)$ . They are also compatible with the ones of one of the structures observed in  $\pi^+\pi^-h_c$  [42]. The large hybrid component (see fig. 7) may explain why it is also observed in this second channel, which would be suppressed by spin symmetry otherwise. It may also be affected by the  $D_1\bar{D}$  threshold (4290 MeV).

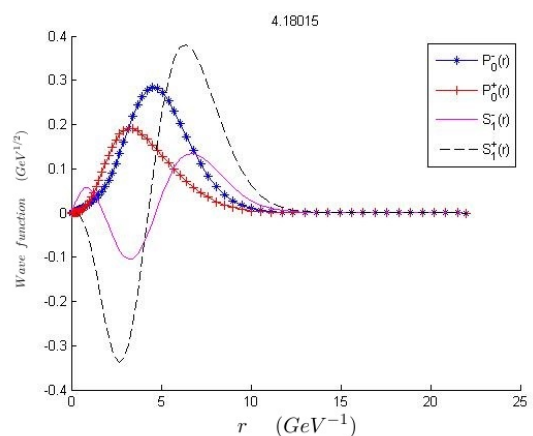


FIG. 7. The wave function of the charmonium  $1^{--} 2d$  state.

- $Y(4274)$  [39] is compatible with our  $1^{++}$  charmonium  $3p$  state (4368 MeV). It may be affected by the  $D_s^*\bar{D}_s^*$  threshold (4224 MeV).
- $X(4350)$  [37] is compatible with our spin one  $2(s/d)_1$  hybrid states (4355 MeV) and charmonium  $3p$  states (4369 MeV).
- $Y(4320)$ ,  $Y(4360)$  and  $Y(4390)$  [37, 41, 42] are compatible with our spin zero  $1^{--}$  hybrid  $2(s/d)_1$  ( $H_1'$ ) state (4366 MeV). Spin symmetry would in principle favor the latter, as it is observed in the  $\pi^+\pi^-h_c$  channel rather than in the  $\pi^+\pi^-J/\psi$  channel. However, the large mixing with spin one charmonium (see table IV and fig. 8) makes the two first ones also acceptable. The absence of any other state in this region in table IV leaves two of them with no assignment. They may be affected by the  $D_0^*\bar{D}^*$  threshold (4407 MeV).

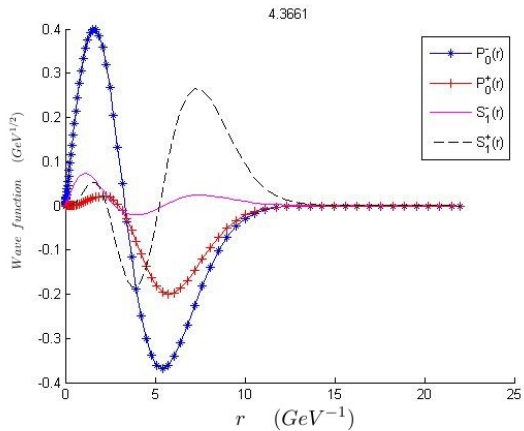


FIG. 8. The wave function of the charmonium  $1^{--} 2(s/d)_1$  state.

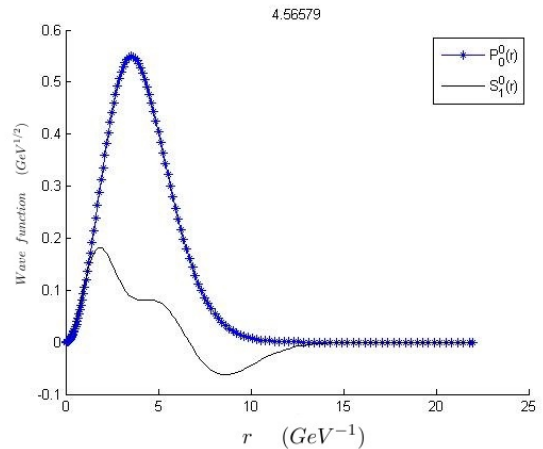


FIG. 9. The wave function of the charmonium  $0^{++} 1p_0$  state.

- $X(4500)$  [39] is compatible with our  $0^{++}$  hybrid  $1p_0$  ( $H_3$ ) state (4566 MeV). However, it mixes very little with spin one charmonium (see table VI and fig. 9), which does not help to understand the observation in the  $J/\psi\phi$  channel. It may be affected by the  $D(2550)\bar{D}^*$  threshold (4557 MeV).

- $Y(4630)$  [37] is compatible with our  $1^{--}$  charmonium  $3d$  state (4559 MeV). It may be affected by the  $D_{s1}\bar{D}_s^*$  thresholds (4572 MeV and 4648 MeV).
- $Y(4660)$  [37] is compatible with our spin zero  $1^{--}$  hybrid  $3(s/d)_1$  ( $H_1''$ ) state (4711 MeV). The mixing with spin one charmonium (see table IV and fig. 10) may explain the observed decays to vector charmonium. It may be affected by the  $D_{s1}\bar{D}_s^*$  and  $D_{s2}^*\bar{D}_s^*$  thresholds (4648 MeV and 4685 MeV).

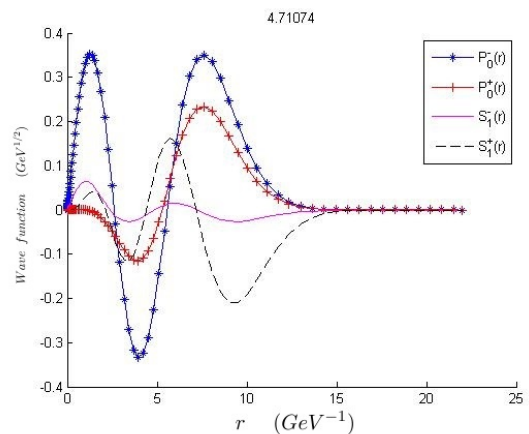


FIG. 10. The wave function of the charmonium  $1^{--} 3(s/d)_1$  state.

- $X(4700)$  [39] is compatible with our  $0^{++}$  charmonium  $4p$  state (4703 MeV).

The assignments above can be visualized in Fig. 11.

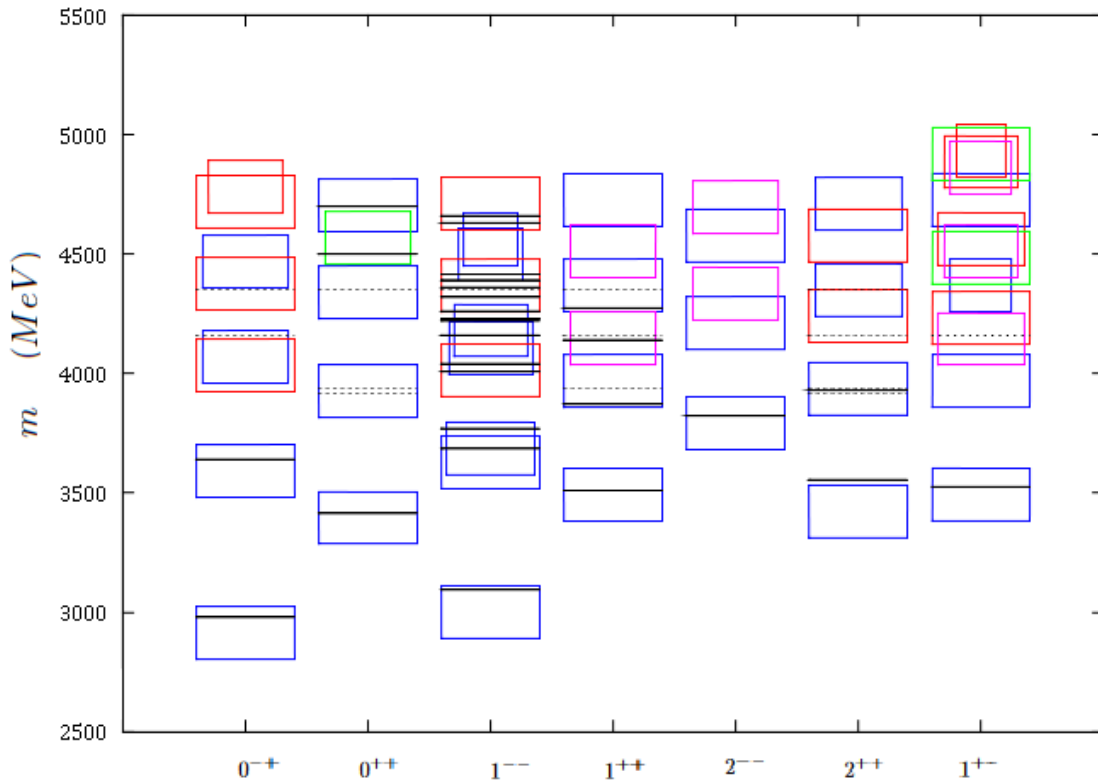


FIG. 11. Charmonium spectrum including hybrids. The height of the boxes corresponds to the error estimated at the end of Sec. IV C. Blue boxes correspond to quarkonium, red boxes to  $(s/d)_1$  and  $(p/f)_2$  hybrids, cyan boxes to  $p_1$  and  $d_2$  hybrids, and green boxes to  $p_0$  hybrids. The black lines are experimental resonances assigned according to the discussion in Sec. VI. Solid (dashed) lines are resonances with a single (multiple) possible assignment(s). The width of the boxes is chosen arbitrarily in order to facilitate identifications.

## B. Bottom

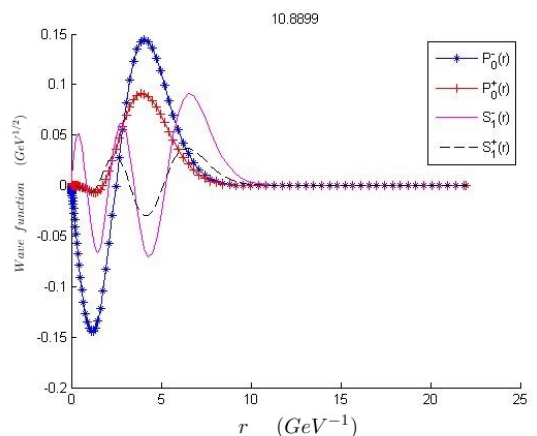


FIG. 12. The wave function of the bottomonium  $1^{--}$   $5s$  state.

- $\Upsilon(10860)$  [37, 43] is compatible with our  $1^{--}$  bottomonium  $5s$  state (10881 MeV). Upon mixing it becomes lighter than the spin zero  $2(s/d)_1$  hybrid nearby (see table XIII and fig. 12). Mixing may also explain the large spin symmetry violating decays to  $\pi^+\pi^-h_b$  [44].

- $Y_b(10890)$  [45] is compatible with our spin zero  $1^{--}$  hybrid  $2(s/d)_1$  state (10890 MeV). Upon mixing becomes heavier than the  $5s$  bottomo-



mium nearby (see table XIII and fig. 13).

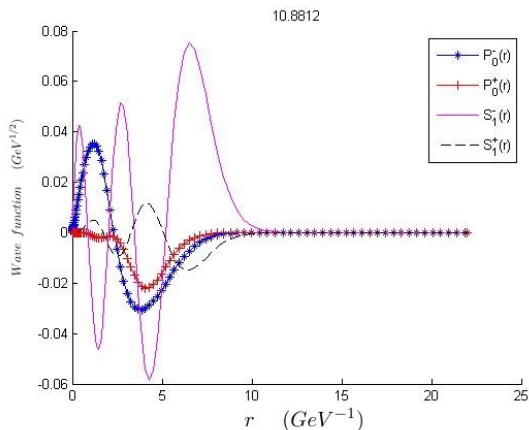


FIG. 13. The wave function of the bottomonium  $1^{--} 2(s/d)_1$  state.

- $\Upsilon(11020)$  [37, 43] is about  $1\sigma$  heavier than our  $1^{--}$  bottomonium  $4d$  state (10942 MeV). It may be affected by the  $B_1\bar{B}$  threshold (11000 MeV).

## VII. DISCUSSION

We have compared our results to other QCD based approaches in section V. We find good agreement with Born-Oppenheimer approaches that have appeared recently in the literature [9, 10], as expected. However the agreement with QCD sum rules and lattice QCD calculations is marginal. The lattice calculations in anisotropic lattices and unphysical quark masses tend to give a heavier hybrid spectrum, both in relativistic implementations of heavy quarks [33, 35] as well as in lattice NRQCD [4]. Nevertheless in [34], a lattice calculation in which both the continuum and the chiral extrapolations are carried out, the three states found that are not identified with known quarkonia fit well in our spectrum. In particular, the  $1^{--}$  state is compatible with the one in our lightest hybrid multiplet.

It is remarkable that the gross features of the experimental charmonium and bottomonium spectrum, including isospin zero XYZ states, can be understood from our results. The main improvement with respect to previous works is that in addition to the Cornell potential for the quarkonium sector and the Born-Oppenheimer potentials for the hybrid sector, we include the leading mixing term between those sectors. The mixing term implies that the actual physical states are a superposition of spin zero (one) hybrids and spin one (zero) quarkonium. This facilitates the identification of certain Y states as hybrids, since otherwise the apparent spin symmetry violating decays were difficult to understand [10]. We would like to

emphasize that the mixing term we use is essentially derived from NRQCD, and hence from QCD. Its short and long distance behavior are obtained in a model independent way. The model dependence comes in through the interpolation we use. We have chosen the sign combination and a value of the free parameter such that a large mixing is favored. It would be very important to have a lattice evaluation of the mixing potential to validate these choices (or otherwise). We have produced formulas (28) that can be easily implemented on the lattice (see for instance [29, 46]).

There appear to be too many known isospin zero  $1^{--}$  charmonium resonances to fit our spectrum in table IV (see also fig. 11). If we assign the  $Y(4008)$  to the  $1(s/d)_1$  state, then  $\psi(4040)$  and  $\psi(4160)$  naturally fall into the  $3s$  and  $2d$  states respectively. However, the  $X(4230)/Y(4220)$  are also candidates for the  $2d$  state. A possible way out would be to disregard  $Y(4008)$ , as it is a very wide resonance that has only been observed by Belle. Then  $\psi(4040)$  would be assigned to the  $1(s/d)_1$  state,  $\psi(4160)$  to the  $3s$  state and  $X(4230)/Y(4220)$  to the  $2d$ . The fact that the  $1(s/d)_1$  state has about a 30% quarkonium component according to the 7th column of table IV (see also fig. 6) may explain why it has been labeled as  $\psi(4040)$ . For the next state,  $2(s/d)_1$ , there are three competing resonances  $Y(4320)$ ,  $Y(4360)$  and  $Y(4390)$ . This makes us suspect that they could well correspond to the same state. Indeed, the decay widths of  $Y(4320)$  and  $Y(4360)$  are compatible and the one of  $Y(4390)$  is less than  $1\sigma$  away. Concerning the masses,  $Y(4320)$  and  $Y(4360)$  are less than  $1\sigma$  away, but  $Y(4390)$  is more than  $5\sigma$  away, which casts some doubts on the suggested identification. Leaving this puzzle aside, there would only be one state to be discovered below the  $Y(4660)$ , the  $3d$  around 4560 MeV.

If we assume for the  $2(s/d)_1$  states the mixing displayed in column 7 of table IV and the decay width in table III for the hybrid component, we obtain

$$\Gamma(Y(4320/4360/4390) \rightarrow h_c + \text{l.h.}) = 14(12) \text{ MeV}, \quad (55)$$

where l.h. stands for light hadrons. Analogously, for the  $X(4230)/Y(4220)$  state we have,

$$\Gamma(X(4230)/Y(4220) \rightarrow h_c + \text{l.h.}) = 17(15) \text{ MeV}. \quad (56)$$

Concerning the  $1^{--}$  bottomonium resonances, all of them fit in our spectrum in table XIII. In addition, there should be three states still to be discovered below the  $\Upsilon(10860)$ , the  $2d$ ,  $1(s/d)_1$  and  $3d$  around 10440 MeV, 10690 MeV and 10710 MeV respectively.

If we take the mixing in column 5 of table XIII and the decay width in table III for the hybrid component, we can also estimate the following decay widths for bottomonium,

$$\begin{aligned} \Gamma(\Upsilon(10860) \rightarrow h_b + \text{l.h.}) &= 3(1) \text{ MeV} \\ \Gamma(Y_b(10890) \rightarrow h_b + \text{l.h.}) &= 13(6) \text{ MeV}. \end{aligned} \quad (57)$$

According to our identifications in section VI, we can infer the quantum numbers of some XYZ states.

- $X(3915)$  should be the  $\chi'_{c0}$  ( $0^{++}$ ).
- $X(3940)$  should be the  $h'_c$  ( $1^{+-}$ ).

It is important to keep in mind that there are further  $1/m_Q$  corrections to the hybrid spectrum beyond those that induce mixing between hybrids and quarkonia we have focused on. In particular, the fine and hyperfine splittings of hybrids may appear at  $\mathcal{O}(1/m_Q)$  rather than at  $\mathcal{O}(1/m_Q^2)$ , as those of quarkonium. Indeed, the following terms are compatible with the symmetries of (3),

$$i\epsilon^{ijk}V^S(r)\text{tr}(H^{i\dagger}[\sigma^k, H^j]), \quad (58)$$

$$i\epsilon^{ijk}V^L(r)\text{tr}(H^{i\dagger}L^k H^j), \quad (59)$$

( $L^k$  is the angular momentum operator) and may appear at  $\mathcal{O}(1/m_Q)$  in the matching to NRQCD.

Before closing, let us briefly discuss the important question on how the lattice potentials we use (fig. 1) may change in the case  $n_f = 3$  (three light quarks). We know that  $\Sigma_g^+$  does not change much and this is also so for  $\Pi_u$  [47], at least up to moderately large distances. Nothing is known about  $\Sigma_u^-$ , but there is no reason to expect a different behavior. Two major qualitative features arise though. The first one is the appearance of heavy-light meson pairs, which amount to roughly horizontal lines at the threshold energies in fig. 1. These states interact with the remaining potentials already at leading order, and may in principle produce important distortions with respect to the  $n_f = 0$  case. In practice, we only know how they cross talk to the  $\Sigma_g^+$  state, and turn out to produce a tiny disturbance to the spectrum, apart from avoiding level crossing [48]. Hence we expect the effects of  $n_f \neq 0$  to be important only when our states are very close to some heavy-light meson pair threshold. This is the reason why we quoted the location of nearby thresholds when identifying our hybrid candidates with XYZ states in section VI. The second one is the appearance of light quark excitations, in addition to the gluon ones, in the static spectrum of fig. 1. They may have different quantum numbers, for instance non zero isospin (in this case they may be relevant to the experimentally discovered charged  $Z$  states). We do not know anything about those and, as pointed out in [49] and more recently emphasized in [9, 50], it would be extremely important to have lattice QCD evaluations of the static energies of light quark excitations. We suspect that light quark excitations with the same quantum numbers as the gluonic ones will only provide small modifications to the hybrid potentials, since they correspond to higher dimensional operators. In this respect, it is significant that tetraquark models have also difficulties to encompass the  $X(4140)$  in their spectrum together

with  $X(4237)$ ,  $X(4500)$  and  $X(4700)$  [51]. In fact, the  $X(4140)$  structure may be due to a threshold enhancement according to some authors [52–54]. This means that tetraquarks with the same quantum numbers as hybrids will in general be hidden in the spectrum of the latter.

## VIII. CONCLUSIONS

We have calculated the charmonium and bottomonium hybrid spectrum in a QCD based approach, including for the first time the mixing with standard charmonium and bottomonium states. The latter leads to enhanced spin symmetry violations, which are instrumental to identify a number of XYZ states as hybrid states. Most of the isospin zero XYZ states fit well in our spectrum, either as hybrids or as standard quarkonium states. We have also estimated several decay widths.

## ACKNOWLEDGMENTS

J.S. thanks Josep Taron for collaboration in the early stages of this work, Jaume Tarrús for discussions and Antonio Pineda for providing the data used in ref. [16]. We have been supported by the Spanish Excellence Network on Hadronic Physics FIS2014-57026-REDT. J.S. also acknowledges support from the 2014-SGR-104 grant (Catalonia), the FPA2013-4657, FPA2013-43425-P, FPA2016-81114-P and FPA2016-76005-C2-1-P projects (Spain).

## Appendix A: Quarkonium

Conventional quarkonium, namely  $Q\bar{Q}$  in a color singlet state, can be described by the Schrödinger equation using the ground state potential  $V_{\Sigma_g^+}(r)$ .

$$h = -\frac{\nabla^2}{m_Q} + V_{\Sigma_g^+}(r). \quad (A1)$$

We approximate  $V_{\Sigma_g^+}(r)$  by the Cornell potential,

$$V_{\Sigma_g^+}(r) \approx -\frac{k_g}{r} + \sigma_g r + E_g^{Q\bar{Q}}, \quad (A2)$$

where we take,

$$k_g = 0.489, \quad \sigma_g = 0.187\text{GeV}^2, \quad (A3)$$

which describes lattice data well, see fig. 2.  $E_g^{Q\bar{Q}}$  will be tuned independently for charmonium and bottomonium. We write the wave-function as  $S(\mathbf{r}) = \frac{R_L(r)}{r} Y_{LM}(\theta, \phi)$ , which leads to the reduced equation:

$$\left(-\frac{1}{m_Q} \frac{\partial^2}{\partial r^2} + \frac{L(L+1)}{m_Q r^2} + V_{\Sigma_g^+}(r)\right) R_L(r) = E R_L(r). \quad (\text{A4})$$

The different eigenvalues of this equation correspond to the energy levels of heavy quarkonium, many of which have been experimentally confirmed for charmonium and bottomonium [37]. We fix  $E_g^{Q\bar{Q}}$  by making the charmonium and bottomonium spectrum to best agree with the respective experimental spin averages. We obtain,

$$E_g^{c\bar{c}} = -0.242 \text{ GeV} \quad E_g^{b\bar{b}} = -0.228 \text{ GeV}. \quad (\text{A5})$$

The table V shows the results in terms of  $M_{Q\bar{Q}} = 2m_Q + E$  for  $Q = c, b$  of eq.(A4) for the lower  $nL$  energy states. It also shows the expectation value of the momentum, the inverse radius, the expected size of the higher order corrections and our error estimate.  $V^{(1)}$ ,  $V_{vd}^{(2)}$  (velocity dependent) and  $V_{vi}^{(2)}$  (velocity independent) depend on  $\Lambda_{\text{QCD}}$  and  $r$ . We take  $\Lambda_{\text{QCD}} = 400$  MeV and estimate them as follows. If  $\Lambda_{\text{QCD}} > 1/\langle r \rangle$  we take them as  $\Lambda_{\text{QCD}}^2 \langle p \rangle^2$  and  $\Lambda_{\text{QCD}}^3$  respectively. If  $\Lambda_{\text{QCD}} < 1/\langle r \rangle$  we take them according to the weak coupling scaling  $\alpha_s^2/\langle r \rangle^2$ ,  $\alpha_s \langle p \rangle^2/\langle r \rangle$  and  $\alpha_s/\langle r \rangle^3$  respectively, where  $\alpha_s$  is the one loop running coupling constant evaluated at the scale  $1/\langle r \rangle$ . The total error is obtained by summing in quadrature these estimates and the relativistic correction to the kinetic energy displayed in the eighth column. We observe that the errors for charmonium are rather large, and are dominated by the velocity dependent potential. We also display the experimental results in the last column.

### Appendix B: Extraction of $g\Lambda'$ and $g\Lambda'''$ from lattice data

$g\Lambda'$  and  $g\Lambda'''$  also appear in the  $1/m_Q^2$  quarkonium potentials [25, 27]. Following the notation of ref. [28], we have that the long distance behavior of the spin-orbit, tensor, and spin-spin potentials reads,

$$\begin{aligned} V_2'(r) &= 2r V_{\mathbf{L}_2 \mathbf{S}_1}^{(1,1)} = -\frac{2c_F g^2 \Lambda^2 \Lambda'}{\kappa r} = -\frac{2c_F g \Lambda'}{r} \\ V_3(r) &= 12 V_{\mathbf{S}_{12}}^{(1,1)} = \frac{2\pi^3 c_F^2 g^2 \Lambda'''^2}{15\kappa^2 r^5} \\ V_4(r) &= 3 V_{\mathbf{S}^2}^{(1,1)} = \frac{\pi^3 c_F^2 g^2 \Lambda'''^2}{30\kappa^2 r^5}. \end{aligned} \quad (\text{B1})$$

We shall take the tree level value for  $c_F$ ,  $c_F = 1$ .

For the spin-orbit potential, a simple interpolation of the expected long and short distance behavior, namely

$$V_2'(r) = \frac{A}{r^2} + \frac{B}{r}, \quad (\text{B2})$$

$nL$	$M_{Q\bar{Q}}$	$\langle p \rangle$	$\frac{1}{\langle r \rangle}$	$\frac{V^{(1)}}{m_Q}$	$\frac{V_{vd}^{(2)}}{m_Q^2}$	$\frac{V_{vi}^{(2)}}{m_Q^2}$	$\frac{p^4}{8m_Q^3}$	$\Delta M_{Q\bar{Q}}$	$E_{exp}$
1s	3068	738	518	54	71	35	12	96	3068
2s	3678	836	259	109	129	30	19	173	3674
3s	4130	935	186	109	162	30	30	199	4039
4s	4517	1019	149	109	192	30	42	227	4421
5s	4865	1097	127	109	223	30	57	256	?
1p	3494	753	317	109	105	30	13	155	3525
2p	3968	871	209	109	140	30	23	182	3927
3p	4369	966	162	109	173	30	34	209	?
4p	4726	1048	135	109	203	30	47	237	?
5p	5055	1136	119	109	239	30	66	272	?
1s	9442	1546	1028	29	37	17	6	50	9445
2s	10009	1408	432	14	22	2	4	26	10017
3s	10356	1494	295	33	38	3	5	50	10355
4s	10638	1594	232	33	43	3	7	54	10579
5s	10885	1692	195	33	48	3	9	59	10876
1p	9908	1268	531	17	19	3	3	26	9900
2p	10265	1386	332	33	32	3	4	46	10260
3p	10553	1504	252	33	38	3	5	51	?
4p	10806	1612	207	33	44	3	7	55	?
5p	11035	1727	180	33	50	3	10	61	?

TABLE V. Masses, average momentum, inverse radius, expected sizes of higher order contributions ( $1/m_Q$  potential,  $1/m_Q^2$  velocity dependent potential,  $1/m_Q^2$  velocity independent potentials,  $1/m_Q^3$  kinetic energy) and estimated error (in MeV) for charmonium (upper) and bottomonium (lower). The error is estimated by summing in quadrature the expected sizes of the higher order contributions (see the text for details on the latter). We have taken  $m_c = 1.47$  GeV and  $m_b = 4.88$  GeV. The experimental numbers are displayed in the last column.

already produces a good fit to data ( $R^2 = 0.998$ , see fig. 14). We obtain  $A = 0.181$  and  $B = 0.295$  in units of  $r_0$ , which translates to  $|g\Lambda'| = 0.059$  GeV. If we restrict ourselves to the longer distance points (from seven to three) and fit the expected long distance behavior only, we obtain worse fits ( $R^2 \lesssim 0.977$ ) with numbers about a 40% higher, which may serve to estimate the error.

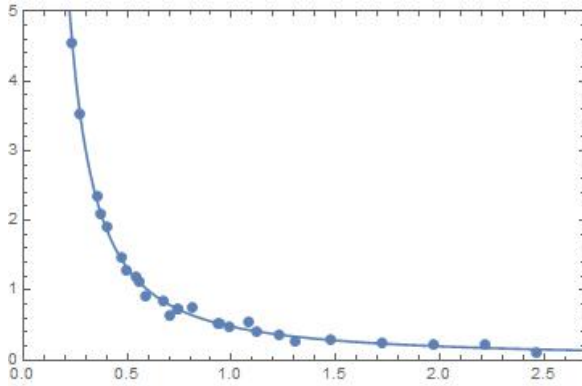


FIG. 14.  $V'_2(r)$  in units of  $r_o^{-2}$  against  $r$  units of  $r_o$ ,  $r_o \sim 0.5$  fm.

For the tensor potential, the following interpolation, which also has the right short and long distance behavior, produces a good fit to data ( $R^2 = 0.996$ , see fig. 15),

$$V_3(r) = \frac{C + Dr}{r^3 + r^6}. \quad (\text{B3})$$

We obtain  $C = 0.191$  and  $D = 1.00$  in units of  $r_o$ , which translates to  $|g\Lambda'''| = 0.230$  GeV. We have checked that if we restrict ourselves to the longer distance points (from seven to three) and fit the expected long distance behavior only, we obtain numbers compatible with the latter within a 35% error.  $|g\Lambda'''|$  may also be obtained from the long distance behavior of the spin-spin potential. However, we have not been able to find a good fit to the data of ref. [28], neither using simple interpolations between the expected short and long distance behavior nor to the expected long distance behavior for the longer distance points (from nine to three).

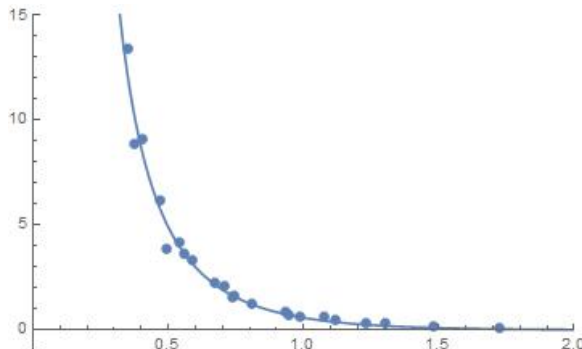


FIG. 15.  $V_3(r)$  in units of  $r_o^{-3}$  against  $r$  in units of  $r_o$ ,  $r_o \sim 0.5$  fm.

### Appendix C: Tensor Spherical Harmonics

We follow the notation of ref. [15]. We define

$$Y_{\mathcal{J}\mathcal{M}}^{ijLJ} = \sum_{\nu=0,\pm 1} C(J1\mathcal{J}; \mathcal{M} - \nu \nu) Y_{\mathcal{J}\mathcal{M}-\nu}^{iL} \chi_{\nu}^j, \quad (\text{C1})$$

where  $Y_{\mathcal{J}\mathcal{M}}^{iL}$  are the vector spherical harmonics,

$$Y_{\mathcal{J}\mathcal{M}}^{iL} = \sum_{\mu=0,\pm 1} C(L1\mathcal{J}; \mathcal{M} - \mu \mu) Y_L^{M-\mu} \chi_{\mu}^i, \quad (\text{C2})$$

where  $Y_L^M$  are the usual spherical harmonics and

$$\chi_{\pm 1} = \mp \frac{1}{\sqrt{2}} \begin{pmatrix} 1 \\ \pm i \\ 0 \end{pmatrix}, \quad \chi_0 = \begin{pmatrix} 0 \\ 0 \\ 1 \end{pmatrix}. \quad (\text{C3})$$

$C(J_1 J_2 J; M_1 M_2)$  are the Clebsch-Gordan coefficients.

### Appendix D: Spectrum

We display in this appendix the tables for the full charmonium and bottomonium spectrum up to  $\mathcal{J} = 2$ , which includes hybrids and quarkonia states, except for the charmonium  $1^{--}$  case that is displayed in table IV.

$NL_J$	$\lambda = 0$	%	$\lambda = 0.6$	%
1p	3.494	0	3.396	7
2p	3.968	0	3.925	1
3p	4.369	0	4.338	0
1p <sub>0</sub>	4.486	100	4.566	98
4p	4.727	0	4.703	9
2p <sub>0</sub>	4.920	100	4.965	94
5p	5.055	0	5.034	1

TABLE VI. Spectrum of charmonium ( $S = 1$ ) and hybrids ( $S = 0$ ):  $0^{++}$  states. Masses are in GeV. The % columns show the fraction of the hybrid components for the mass states in the previous column. The mixing potentials are fixed to  $V_S^{\Pi}[+-]$  and  $V_S^{\Sigma}[++]$ .  $m_c = 1.47$  GeV.

$NL_J$	$\lambda = 0$	%	$\lambda = 0.6$	%
1p	3.494	0	3.492	0
2p	3.968	0	3.967	0
1p <sub>1</sub>	4.145	100	4.146	100
3p	4.369	0	4.368	0
2p <sub>1</sub>	4.511	100	4.512	100
4p	4.727	0	4.726	0
3p <sub>1</sub>	4.863	100	4.863	99
5p	5.055	0	5.055	1

TABLE VII. Same as in table VI for  $1^{++}$  states.

$NL_J$	$\lambda = 0$	%	$\lambda = 0.6$	%
1s	3.068	0	2.913	7
2s	3.678	0	3.591	8
1(s/d) <sub>1</sub>	4.011	100	4.033	99
3s	4.131	0	4.069	1
2(s/d) <sub>1</sub>	4.355	100	4.375	92
4s	4.512	0	4.468	7
3(s/d) <sub>1</sub>	4.692	100	4.719	99
4(s/d) <sub>1</sub>	4.718	100	4.781	96
5s	4.865	0	4.823	0
5(s/d) <sub>1</sub>	5.043	100	5.055	96

TABLE X. Spectrum of charmonium ( $S = 0$ ) and charmonium hybrids ( $S = 1$ ):  $0^{-+}$  states. Masses are in GeV. The % columns show the fraction of the hybrid components for the mass states in the previous column. The mixing potentials are fixed to  $V_S^{\Pi}[\pm-]$  and  $V_S^{\Sigma}[\pm+]$ .  $m_c = 1.47$  GeV.

$NL_J$	$\lambda = 0$	%	$\lambda = 0.6$	%
1p	3.494	0	3.424	5
2p	3.968	0	3.937	7
1f	4.047	0	3.981	11
1(p/f) <sub>2</sub>	4.231	100	4.240	81
3p	4.369	0	4.350	0
2f	4.428	0	4.391	77
2(p/f) <sub>2</sub>	4.563	100	4.579	53
4p	4.727	0	4.709	3
3f	4.775	0	4.752	11
3(p/f) <sub>2</sub>	4.886	100	4.909	78
4(p/f) <sub>2</sub>	4.923	100	4.952	94
5p	5.055	0	5.040	4

TABLE VIII. Same as in table VI for  $2^{++}$  states.

$NL_J$	$\lambda = 0$	%	$\lambda = 0.6$	%
1p	3.494	0	3.333	9
2p	3.968	0	3.901	2
1p <sub>1</sub>	4.145	100	4.146	100
1(p/f) <sub>2</sub>	4.231	100	4.242	99
3p	4.369	0	4.320	1
1p <sub>0</sub>	4.486	100	4.511	98
2p <sub>1</sub>	4.511	100	4.526	100
2(p/f) <sub>2</sub>	4.563	100	4.590	95
4p	4.727	0	4.686	8
3p <sub>1</sub>	4.863	100	4.863	100
3(p/f) <sub>2</sub>	4.886	100	4.901	99
2p <sub>0</sub>	4.920	100	4.936	95
4(p/f) <sub>2</sub>	4.923	100	4.959	100
5p	5.055	0	5.020	7

TABLE XI. Same as in table X for  $1^{+-}$  states.

$NL_J$	$\lambda = 0$	%	$\lambda = 0.6$	%
1d	3.793	0	3.792	0
2d	4.210	0	4.209	1
1d <sub>2</sub>	4.334	100	4.335	100
3d	4.579	0	4.578	0
2d <sub>2</sub>	4.693	100	4.694	99
4d	4.916	0	4.915	0
3d <sub>2</sub>	5.036	100	5.037	100

TABLE IX. Same as in table VI for  $2^{--}$  states.

$NL_J$	$\lambda = 0$	%	$\lambda = 0.6$	%
1d	3.793	0	3.721	6
1(s/d) <sub>1</sub>	4.011	100	4.014	75
2d	4.210	0	4.199	80
1d <sub>2</sub>	4.334	100	4.335	100
2(s/d) <sub>1</sub>	4.355	100	4.353	73
1(d/g) <sub>3</sub>	4.435	100	4.443	100
3d	4.579	0	4.571	11
3(s/d) <sub>1</sub>	4.692	100	4.690	97
2d <sub>2</sub>	4.693	100	4.694	98
4(s/d) <sub>1</sub>	4.718	100	4.713	96
2(d/g) <sub>3</sub>	4.763	100	4.774	90
4d	4.916	0	4.911	27
3d <sub>2</sub>	5.036	100	5.037	95
5(s/d) <sub>1</sub>	5.043	100	5.084	98

TABLE XII. Same as in table X for  $2^{-+}$  states.

$NL_J$	$\lambda = 0$	%	$\lambda = 0.6$	%
1s	9.442	0	9.441	0
2s	10.009	0	10.000	2
1d	10.155	0	10.133	2
3s	10.356	0	10.352	0
2d	10.454	0	10.440	2
4s	10.638	0	10.635	1
1(s/d) <sub>1</sub>	10.690	100	10.688	79
3d	10.712	0	10.713	56
2(s/d) <sub>1</sub>	10.885	100	10.881	17
5s	10.886	0	10.890	75
4d	10.947	0	10.942	11
3(s/d) <sub>1</sub>	11.084	100	11.086	98

TABLE XIII. Spectrum of bottomonium ( $S = 1$ ) and hybrids ( $S = 0$ ):  $1^{--}$  states. Masses are in GeV. The % columns show the fraction of the hybrid components for the mass states in the previous column. The mixing potentials are fixed to  $V_S^{\Pi}[+-]$  and  $V_S^{\Sigma}[++]$ .  $m_b = 4.88$  GeV.

$NL_J$	$\lambda = 0$	%	$\lambda = 0.6$	%
1p	9.908	0	9.907	0
2p	10.265	0	10.264	0
3p	10.553	0	10.553	0
4p	10.806	0	10.805	0
1p <sub>0</sub>	11.011	100	11.013	99

TABLE XIV. Same as in table XIII for  $0^{++}$  states.

$NL_J$	$\lambda = 0$	%	$\lambda = 0.6$	%
1p	9.908	0	9.908	0
2p	10.265	0	10.265	0
3p	10.553	0	10.553	0
1p <sub>1</sub>	10.761	100	10.761	99
1p	10.806	0	10.806	0
2p <sub>1</sub>	10.970	100	10.970	99
5p	11.034	0	11.035	0

TABLE XV. Same as in table XIII for  $1^{++}$  states.

$NL_J$	$\lambda = 0$	%	$\lambda = 0.6$	%
1p	9.908	0	9.898	1
2p	10.265	0	10.258	1
1f	10.348	0	10.331	2
3p	10.553	0	10.549	0
2f	10.615	0	10.603	5
4p	10.806	0	10.801	13
1(p/f) <sub>2</sub>	10.819	100	10.820	91
3f	10.855	0	10.851	32
2(p/f) <sub>2</sub>	11.005	100	11.009	80

TABLE XVI. Same as in table XIII for  $2^{++}$  states.

$NL_J$	$\lambda = 0$	%	$\lambda = 0.6$	%
1d	10.155	0	10.155	0
2d	10.453	0	10.454	0
3d	10.712	0	10.713	0
1d <sub>2</sub>	10.870	100	10.870	100
4d	10.947	0	10.947	0
2d <sub>2</sub>	11.074	100	11.074	100

TABLE XVII. Same as in table XIII for  $2^{--}$  states.

$NL_J$	$\lambda = 0$	%	$\lambda = 0.6$	%
1s	9.442	0	9.427	1
2s	10.009	0	9.987	3
3s	10.356	0	10.343	1
4s	10.638	0	10.629	3
1(s/d) <sub>1</sub>	10.690	100	10.693	99
5s	10.886	0	10.877	16
2(s/d) <sub>1</sub>	10.885	100	10.890	81
3(s/d) <sub>1</sub>	11.084	100	11.086	95

TABLE XVIII. Spectrum of bottomonium ( $S = 0$ ) and bottomonium hybrids ( $S = 1$ ):  $0^{-+}$  states. Masses are in GeV. The % columns show the fraction of the hybrid components for the mass states in the previous column. The mixing potentials are fixed to  $V_S^{\Pi}[+-]$  and  $V_S^{\Sigma}[++]$ .  $m_b = 4.88$  GeV.

$NL_J$	$\lambda = 0$	%	$\lambda = 0.6$	%
1p	9.908	0	9.886	2
2p	10.265	0	10.249	2
3p	10.553	0	10.543	0
1p <sub>1</sub>	10.761	100	10.761	100
4p	10.806	0	10.798	1
1(p/f) <sub>2</sub>	10.819	100	10.820	100
2p <sub>1</sub>	10.970	100	10.969	100
1p <sub>0</sub>	11.011	100	11.006	100

TABLE XIX. Same as in table XVIII for  $1^{+-}$  states.

$NL_J$	$\lambda = 0$	%	$\lambda = 0.6$	%
1d	10.155	0	10.144	2
2d	10.454	0	10.444	3
1(s/d) <sub>1</sub>	10.690	100	10.685	82
3d	10.712	0	10.717	52
1d <sub>2</sub>	10.870	100	10.870	100
2(s/d) <sub>1</sub>	10.885	100	10.886	94
1(d/g) <sub>1</sub>	10.935	100	10.937	99
4d	10.947	0	10.945	13
2d <sub>2</sub>	11.074	100	11.074	99

TABLE XX. Same as in table XVIII for  $2^{-+}$  states.

- 
- [1] S. L. Olsen, PoS Bormio 050 (2015) [arXiv:1511.01589 [hep-ex]].
- [2] W. E. Caswell and G. P. Lepage, Phys. Lett. **167B**, 437 (1986). doi:10.1016/0370-2693(86)91297-9
- [3] G. T. Bodwin, E. Braaten and G. P. Lepage, Phys. Rev. D **51**, 1125 (1995) Erratum: [Phys. Rev. D **55**, 5853 (1997)] doi:10.1103/PhysRevD.55.5853, 10.1103/PhysRevD.51.1125 [hep-ph/9407339].
- [4] K. J. Juge, J. Kuti and C. J. Morningstar, Phys. Rev. Lett. **82**, 4400 (1999) doi:10.1103/PhysRevLett.82.4400 [hep-ph/9902336].
- [5] G. Chiladze, A. F. Falk and A. A. Petrov, Phys. Rev. D **58**, 034013 (1998) doi:10.1103/PhysRevD.58.034013 [hep-ph/9804248].
- [6] N. Brambilla, A. Pineda, J. Soto and A. Vairo, Nucl. Phys. B **566**, 275 (2000) doi:10.1016/S0550-3213(99)00693-8 [hep-ph/9907240].
- [7] K. J. Juge, J. Kuti and C. Morningstar, Phys. Rev. Lett. **90**, 161601 (2003) doi:10.1103/PhysRevLett.90.161601 [hep-lat/0207004].
- [8] S. Perantonis and C. Michael, Nucl. Phys. B **347**, 854 (1990). doi:10.1016/0550-3213(90)90386-R
- [9] E. Braaten, C. Langmack and D. H. Smith, Phys. Rev. D **90**, no. 1, 014044 (2014) doi:10.1103/PhysRevD.90.014044 [arXiv:1402.0438 [hep-ph]].
- [10] M. Berwein, N. Brambilla, J. Tarrús Castellà and A. Vairo, Phys. Rev. D **92**, no. 11, 114019 (2015) doi:10.1103/PhysRevD.92.114019 [arXiv:1510.04299 [hep-ph]].
- [11] R. Onocala and J. Soto, arXiv:1611.04761 [hep-ph].
- [12] A. Pineda and J. Soto, Nucl. Phys. Proc. Suppl. **64**, 428 (1998) doi:10.1016/S0920-5632(97)01102-X [hep-ph/9707481].
- [13] M. Luscher and P. Weisz, JHEP **0207**, 049 (2002) doi:10.1088/1126-6708/2002/07/049 [hep-lat/0207003].
- [14] M. Luscher and P. Weisz, JHEP **0407**, 014 (2004) doi:10.1088/1126-6708/2004/07/014 [hep-th/0406205].
- [15] A. Galindo and P. Pascual, *Quantum Mechanics I* (Springer Berlin Heidelberg, 1990) 334-338.
- [16] G. S. Bali and A. Pineda, Phys. Rev. D **69**, 094001 (2004) doi:10.1103/PhysRevD.69.094001 [hep-ph/0310130].
- [17] R. Onocala, *Study of XYZ mesons as heavy hybrid mesons in the Born-Oppenheimer approximation*, M.Sc. Thesis, Universitat de Barcelona, July 2016.
- [18] N. Brambilla, A. Pineda, J. Soto and A. Vairo, Rev. Mod. Phys. **77**, 1423 (2005) doi:10.1103/RevModPhys.77.1423 [hep-ph/0410047].
- [19] E. Braaten, C. Langmack and D. H. Smith, Phys. Rev. Lett. **112**, 222001 (2014) doi:10.1103/PhysRevLett.112.222001 [arXiv:1401.7351 [hep-ph]].
- [20] N. Brambilla, A. Pineda, J. Soto and A. Vairo, Phys. Rev. D **63**, 014023 (2001) doi:10.1103/PhysRevD.63.014023 [hep-ph/0002250].
- [21] A. Pineda and A. Vairo, Phys. Rev. D **63**, 054007 (2001) Erratum: [Phys. Rev. D **64**, 039902 (2001)] doi:10.1103/PhysRevD.64.039902, 10.1103/PhysRevD.63.054007 [hep-ph/0009145].
- [22] E. Eichten and F. Feinberg, Phys. Rev. D **23**, 2724 (1981). doi:10.1103/PhysRevD.23.2724
- [23] G. S. Bali, Phys. Rept. **343**, 1 (2001) doi:10.1016/S0370-1573(00)00079-X [hep-ph/0001312].
- [24] N. Brambilla, D. Eiras, A. Pineda, J. Soto and A. Vairo, Phys. Rev. D **67**, 034018 (2003) doi:10.1103/PhysRevD.67.034018 [hep-ph/0208019].
- [25] G. Perez-Nadal and J. Soto, Phys. Rev. D **79**, 114002 (2009) doi:10.1103/PhysRevD.79.114002 [arXiv:0811.2762 [hep-ph]].
- [26] J. B. Kogut and G. Parisi, Phys. Rev. Lett. **47**, 1089 (1981). doi:10.1103/PhysRevLett.47.1089
- [27] N. Brambilla, M. Groher, H. E. Martinez and A. Vairo, Phys. Rev. D **90**, no. 11, 114032 (2014) doi:10.1103/PhysRevD.90.114032 [arXiv:1407.7761 [hep-ph]].
- [28] Y. Koma and M. Koma, PoS LAT **2009**, 122 (2009) [arXiv:0911.3204 [hep-lat]].
- [29] Y. Koma and M. Koma, Nucl. Phys. B **769**, 79 (2007) doi:10.1016/j.nuclphysb.2007.01.033 [hep-lat/0609078].
- [30] L. Liu *et al.* [Hadron Spectrum Collaboration], JHEP **1207**, 126 (2012) doi:10.1007/JHEP07(2012)126 [arXiv:1204.5425 [hep-ph]].
- [31] A. Pineda, JHEP **0106**, 022 (2001) doi:10.1088/1126-6708/2001/06/022 [hep-ph/0105008].
- [32] X. Liao and T. Manke, hep-lat/0210030.
- [33] G. K. C. Cheung *et al.* [Hadron Spectrum Collaboration], JHEP **1612**, 089 (2016) doi:10.1007/JHEP12(2016)089 [arXiv:1610.01073 [hep-lat]].
- [34] K. Cichy, M. Kalinowski and M. Wagner, Phys. Rev. D **94**, no. 9, 094503 (2016) doi:10.1103/PhysRevD.94.094503 [arXiv:1603.06467 [hep-lat]].
- [35] X. Liao and T. Manke, Phys. Rev. D **65**, 074508 (2002) doi:10.1103/PhysRevD.65.074508 [hep-lat/0111049].
- [36] W. Chen, R. T. Kleiv, T. G. Steele, B. Bulthuis, D. Harnett, J. Ho, T. Richards and S. L. Zhu, JHEP **1309**, 019 (2013) doi:10.1007/JHEP09(2013)019 [arXiv:1304.4522 [hep-ph]].
- [37] C. Patrignani *et al.* [Particle Data Group], Chin. Phys. C **40**, no. 10, 100001 (2016). doi:10.1088/1674-1137/40/10/100001
- [38] Z. Q. Liu *et al.* [Belle Collaboration], Phys. Rev. Lett. **110**, 252002 (2013) doi:10.1103/PhysRevLett.110.252002 [arXiv:1304.0121 [hep-ex]].
- [39] R. Aaij *et al.* [LHCb Collaboration], Phys. Rev. Lett. **118**, no. 2, 022003 (2017) doi:10.1103/PhysRevLett.118.022003 [arXiv:1606.07895 [hep-ex]].
- [40] R. E. Mitchell [BESIII Collaboration], arXiv:1611.04669 [hep-ex].

- [41] M. Ablikim *et al.* [BESIII Collaboration], arXiv:1611.01317 [hep-ex].
- [42] M. Ablikim *et al.* [BESIII Collaboration], arXiv:1610.07044 [hep-ex].
- [43] D. Santel *et al.* [Belle Collaboration], Phys. Rev. D **93**, no. 1, 011101 (2016) doi:10.1103/PhysRevD.93.011101 [arXiv:1501.01137 [hep-ex]].
- [44] R. Mizuk *et al.* [Belle Collaboration], Phys. Rev. Lett. **117**, no. 14, 142001 (2016) doi:10.1103/PhysRevLett.117.142001 [arXiv:1508.06562 [hep-ex]].
- [45] I. Adachi *et al.* [Belle Collaboration], arXiv:0808.2445 [hep-ex].
- [46] Y. Koma, M. Koma and H. Wittig, Phys. Rev. Lett. **97**, 122003 (2006) doi:10.1103/PhysRevLett.97.122003 [hep-lat/0607009].
- [47] G. S. Bali *et al.* [TXL and T(X)L Collaborations], Phys. Rev. D **62**, 054503 (2000) doi:10.1103/PhysRevD.62.054503 [hep-lat/0003012].
- [48] G. S. Bali *et al.* [SESAM Collaboration], Phys. Rev. D **71**, 114513 (2005) doi:10.1103/PhysRevD.71.114513 [hep-lat/0505012].
- [49] N. Brambilla, A. Vairo, A. Polosa and J. Soto, Nucl. Phys. Proc. Suppl. **185**, 107 (2008). doi:10.1016/j.nuclphysbps.2008.10.011
- [50] E. Braaten, Phys. Rev. Lett. **111**, 162003 (2013) doi:10.1103/PhysRevLett.111.162003 [arXiv:1305.6905 [hep-ph]].
- [51] A. Esposito, A. Pilloni and A. D. Polosa, Phys. Rept. **668**, 1 (2016) doi:10.1016/j.physrep.2016.11.002 [arXiv:1611.07920 [hep-ph]].
- [52] E. van Beveren and G. Rupp, arXiv:0906.2278 [hep-ph].
- [53] X. H. Liu, Phys. Lett. B **766**, 117 (2017) doi:10.1016/j.physletb.2017.01.008 [arXiv:1607.01385 [hep-ph]].
- [54] P. G. Ortega, J. Segovia, D. R. Entem and F. Fernández, Phys. Rev. D **94**, no. 11, 114018 (2016) doi:10.1103/PhysRevD.94.114018 [arXiv:1608.01325 [hep-ph]].